BAW-10094, Rev 3
February 1981

Babcock & Wilcox Revisions to THETA1-B, a Computer Code for Nuclear Reactor Core Thermal Analysis (IN-1445)

— Revision 3 —

BABCOCK & WILCOX
Nuclear Power Group
Nuclear Power Generation Division
P. O. Box 1260
Lynchburg, Virginia 24505

Babcock & Wilcox

ACKNOWLEDGMENTS

The authors are indebted to K. R. Katsma and M. L. Uptmor who converted the CINDA-3G thermal analyzer code for use on the IBM-360/75 computer at the National Reactor Testing Station, to C. F. Carmichael and J. R. Larson for many helpful suggestions, and to E. D. Hughes for his advice concerning CHF correlations.

ABSTRACT

A digital computer code, THETA1-B, was developed to study the thermal response characteristics of a nuclear fuel rod subjected to a postulated loss-of-coolant accident environment. This code was developed as part of the Loss-of-Coolant Accident Analysis Program currently being conducted at the National Reactor Testing Station by Idaho Nuclear Corporation for the Atomic Energy Commission.

The energy equations for both the fuel rod and the adjacent fluid channel are solved. A heat transfer model is employed to link the solutions of the two energy equations. This model has been developed on the basis of heat transfer correlations available in the open literature.

The code has the capability of modeling electrically heated test elements. This feature allows the postulated heat transfer model to be evaluated in terms of experimental heat transfer data obtained during decompression tests.

SUMMARY

A digital computer code, THETA1-B (THermal Energy Transport Analysis, Version 1-B) has been written to solve the equations that describe the thermal energy transfer processes that would occur if a nuclear fuel rod were subjected to a loss-of-coolant accident (LOCA) environment. THETA1-B solves the two-dimensional diffusion equation for a single fuel rod and the one-dimensional conservation of energy equation for the associated fluid channel. The two solutions are linked together at the fuel rod-fluid interface by the boundary conditions of surface temperature and heat flux.

The fuel rod may be modeled by using up to 20 axial levels and up to 50 radial regions. Radial conduction paths are included at all axial levels and axial conduction paths may be included or excluded as desired. The diffusion equation that describes the conduction in the fuel rod is solved by the CINDA-3G thermal analyzer code, which is part of THETA1-B.

The fluid channel is modeled by a number of axial regions corresponding to those used in the fuel rod model. The energy balance in the fluid is described by the one-dimensional conservation of energy equation for a nonhomogeneous two-phase flow situation. Several numerical differencing schemes were developed to solve the energy equation. The techniques employed and the relative merits of each scheme are discussed.

The heat transfer model considers the following heat transfer regimes: forced convection in subcooled liquid and superheated vapor, nucleate boiling, forced convection vaporization, transition boiling, and stable film boiling. More than one option for choice of heat transfer correlation exists for several of the heat transfer regimes. Also a number of critical heat flux correlations have been incorporated into the heat transfer model.

At high temperatures, the Zircaloy cladding will react with steam. This reaction is described by a parabolic rate equation provided sufficient steam is available for the reaction. If sufficient steam is not available, then a steam limiting calculation is performed. The metal-water reaction computation may be included or deleted as desired.

The code may also be used to model electrically heated test elements commonly used to stimulate nuclear fuel rods. This feature is useful in analyzing the thermal response of electrically heated rods that are used in out-of-pile decompression heat transfer experiments.

NOMENCLATURE

A	Cross sectional area, ft^2
C_p	Specific heat, Btu/lbm-°F
C_j^n	Thermal capacitance, Btu/°F
D	Diameter, in.
d_c	Cladding diameter, in.
d_f	Fuel diameter, in.
D_e	Equivalent diameter, in.
Dz	Length of control volume, ft.
E	Modulus of elasticity, psi
g	Local acceleration of gravity, ft/s^2
g_i	Temperature jump distance, in.
g_o	Gravitational constant, ft-lbm/lbf-s^2
G	Mass flux, lbm/s-ft^2
G_{ij}^n	Thermal conductance, Btu/ s-°F
H	Meyer hardness number, psi
h^{ij}	Heat transfer coefficient, Btu/ft^2-s-°F
h	Thermodynamic enthalpy, Btu/lbm
h'	Flow enthalpy (defined by equation 11), Btu/lbm
k	Thermal conductivity, Btu/ft-s-°F
K_s	Slip velocity ratio (defined by equation 13)
ℓ	Length between nodal locations, ft
L	Length, in.
p	Pressure, psia
Pr	Prandtl number
q'''	Power density, Btu/ft^3-s
$\dot{q}$	Heat flux, Btu/ft^2-s
Q	Volumetric flow rate, ft^3/s
Q_j^n	Power generation rate, Btu/s
r	Radius, ft

R	Radius of fuel rod, ft
Re	Reynolds number
t	Time, seconds(s)
Δt	Time step, s
T	Temperature, F
ΔT_{sat}	Wall temperature minus saturation temperature, F
V	Volume, ft^3
v	Specific volume, ft^3/lbm
x	Thermodynamic quality
x´	Mass flow fraction (defined by equation 12)
z	Axial distance, ft

Greek Letters

α	Void fraction
α_f	Coefficient of thermal expansion for fuel, 1/°F
α_c	Coefficient of thermal expansion for cladding, 1/°F
ε	Emissivity (-)
λ	Mean free path, cm
μ	Absolute viscosity, lbm/ft-s
μ	Poisson's ratio (-)
ρ	Density, lbm/ft^3
σ	Surface tension, lbf/ft
ϕ	Heat flux × wetted perimeter of fuel rod ÷ cross-sectional flow area of channel, Btu/ft^3-s

Superscripts

n	Quantity is evaluated at the nth time step

Subscripts

CHF	Critical heat flux conditions
f	Evaluated at saturated liquid conditions
fg	Refers to phase change by evaporation
flow	Refers to cross-sectional flow area
g	Evaluated at saturated vapor conditions
HE	Based on heated perimeter
HY	Based on hydraulic perimeter
in	Inlet
j	Refers to axial position

J	Total number of axial levels
NU	Nonuniform
U	Uniform
v	Superheated vapor
w	Wall

CONTENTS

1

CONTENTS (Cont'd)

List of Figures

THETA1-B, A COMPUTER CODE FOR NUCLEAR REACTOR CORE THERMAL ANALYSIS

I. INTRODUCTION

The primary objective of the Loss-of-Coolant Accident Analysis Program [1] is to provide the Atomic Energy Commission and the nuclear reactor industry with experimentally verified analytical techniques for analyzing a loss-of-coolant accident (LOCA) situation. The THETA1-B digital computer code was developed as part of this program and is designed to study the thermal response of a nuclear fuel rod during the decompression and heat-up phases of a LOCA. This thermal response analytical capability is required in order to determine the mechanical integrity of the fuel rod which is dependent on the maximum cladding temperature reached during the decompression.

The fluid dynamic and heat transfer processes occurring in a nuclear reactor core during a LOCA are extremely complex. To accurately determine the thermal response of the fuel rods, the complete set of conservation equations must be solved in detail throughout the entire primary system. Currently a code of sufficient complexity does not exist. Therefore, common practice in the nuclear reactor industry has been to determine the fluid behavior for the complete reactor primary loop by using a code such as RELAP3 [2] in which the coupled set of conservation equations are solved but not in great detail. Then the core fluid conditions, as determined by the primary-loop code, are used as input to the core heat transfer code and the detailed thermal response of a single fuel rod is obtained. THETA1-B is a detailed core heat transfer code of this nature.

THETA1-B is currently being used in the preliminary steady state design of the nuclear core to be used in the Loss-of-Fluid Test (LOFT) Program [3], which is part of the Water Reactor Safety Program of the Atomic Energy Commission. The code is also to be used to predict the thermal response of the LOFT nuclear core during decompression tests.

In addition to the capability of analyzing the response of a nuclear rod for a postulated LOCA situation, THETA1-B also has the capability of analyzing the behavior of electrically heated test elements used to simulate nuclear rods during decompression heat transfer experiments.

The basic heat transfer model and the assumptions inherent in this model and code limitations are delineated in this report. Numerical techniques used to solve the equations describing the model are discussed and a typical transient cladding temperature response curve is analyzed. Input requirements are also described.

II. DESCRIPTION OF MATHEMATICAL MODEL

The THETA1-B code solves the two-dimensional diffusion equation (energy equation) for a single fuel rod and the one-dimensional conservation of energy equation for the coolant in the surrounding channel. The solutions of the two energy equations are linked together through the heat flux which is determined by a heat transfer model.

The boundary conditions needed in the THETA1-B code are obtained from a code such as RELAP3 [2] which solves the fluid dynamics equation for the complete reactor primary system.

1. GENERAL MODEL DESCRIPTION

The diffusion equation which describes the conduction phenomena in the fuel rod is solved by an electrical analogy technique. The resulting resistance-capacitance (RC) network is solved by the CINDA-3G [4] (Chrysler Improved Numerical Differencing Analyzer for 3rd Generation Computers) thermal analyzer code.

The energy balance on the fluid is described by the one-dimensional conservation of energy equation for a nonhomogeneous one-component two-phase flow situation. Various numerical differencing techniques were developed during the course of the project to solve this equation. The first schemes developed were either unstable or inaccurate. Ultimately a stable and accurate scheme based on the method of characteristics was developed.

A heat transfer model provides the boundary conditions required during the solution of the energy equations in both the fuel rod and fluid. The local thermodynamic fluid properties and the local cladding surface temperature are used to determine the magnitude of the heat flux and the appropriate heat transfer regime.

Both steady state and transient solutions may be obtained by using THETA1-B. A sequence of steady state solutions may be obtained with a single data deck. However, only one input parameter may be varied in each set of solutions. This feature is described more fully in the data input requirements section. A transient solution is always preceded by a steady state initialization.

The code was designed for use more as a development tool than as a production code. Thus, a number of geometric and heat transfer options are available rather than one fixed computational procedure. An additional feature allows any of the existing heat transfer correlations to be replaced at the discretion of the user. The thermal response of electrically heated fuel rod simulators may also be obtained.

2. FUEL ROD CONDUCTION MODEL

The heat conduction process occurring in the fuel rod is assumed to be two-dimensional; axial and radial conduction are allowed but azimuthal conduction is ignored. The resulting conduction equation

$$\rho C_p \frac{\partial T}{\partial t} = k \frac{1}{r} \frac{\partial}{\partial r} \left(r \frac{\partial T}{\partial r}\right) + k \frac{\partial^2 T}{\partial z^2} + q''' \qquad (1)$$

is solved through use of an electrical analogy technique[a]. The rod is first divided into a number of finite regions. An RC network is used to represent the fuel rod. The regions are represented in the network by nodes that are positioned in the geometric center of the regions. Each node has a thermal capacitance value associated with it. The thermal resistance in the fuel rod is represented by resistances that are placed between nodes. The CINDA-3G [4] thermal analyzer code is used to solve the set of equations that describes the thermal network.

The following initial and boundary conditions are required for the solution of the conduction equation:

$$q''' (t) = f_1(t) \qquad (2a)$$

$$T(R,z,0) = f_2(z,0) \qquad (2b)$$

$$\dot{q} (R,z,t) = f_3(z,t) \qquad (2c)$$

The quantity $f_1(t)$ for $t = 0$ is equal to the total power generated per second divided by the volume of the fuel in the rod. The decay power term $f_1(t)$ is determined by the reactor kinetics model in a reactor system thermal hydraulics code. In addition to the power generation rate, the radial power profile in the fuel pellet and the axial power profile along the fuel rod length must be specified.

The surface temperature $f_2(z, 0)$ is not known a priori but is obtained as part of the overall steady state solution. During steady state initialization $f_2(z, 0)$ is obtained from an iterative procedure.

The surface heat flux $f_3(z, t)$ is determined during the transient solution. The manner in which this quantity is obtained is described in Section III.

2.1 Fuel Rod Control Volume Description

First the fuel rod is divided into a number of small three-dimensional control volumes. A maximum of 50 radial divisions in both the fuel pellet and cladding is allowed. Also 20 axial levels are allowed. In the axial direction the rod may be divided into a selected number of increments of equal length or into a number of increments of unequal length.

---

[a] The nomenclature in this and succeeding equations is defined in the front of this report.

Several options are available for describing the shape of the control volumes in the radial direction. The control volume shape in the fuel pellets may be equal thickness annuli, equal cross-sectional area annuli, or some alternative pattern as specified by the user. The equal thickness annulus case is the better of the two standard options in that the control volume interfaces are positioned uniformly in the radial direction across the fuel pellet and consequently the temperature distribution is based on a uniformly spaced radial grid.

The control volume pattern in the cladding material is different from that in the fuel pellet. In general, the interfaces are positioned uniformly in the radial direction; that is, the interfaces are positioned such that the annular regions, or control volumes, are of equal thickness. If the cladding is to be represented by two volumes the interface is positioned such that the thickness of the outermost control volume is one quarter the thickness of the sum of the thicknesses of the two control volumes. If three or more control volumes are used in the cladding, the thickness of the volumes are determined in the following manner. If N control volumes are desired the cladding is first divided into N-1 equal thickness annuli. Then the outer region is divided into two control volumes having a three-to-one thickness ratio as described for the two-volume case. This choice of spacing allows a node to be positioned quite close to the cladding outer surface without adversely affecting the numerical stability of the network solution. This pattern is automatically used in the cladding if either of the two standard fuel pellet patterns is chosen. However, if the interface locations have been specified otherwise in the fuel pellet, they must also be specified in the cladding. The control volume pattern options in the fuel pellet and cladding are shown in Figures 1 and 2, respectively.

Once the number of axial and radial regions and the geometric pattern have been selected the fuel rod can be represented schematically in a thermal network format[4]. The control volumes are represented as nodes in the network and a thermal capacitance value is assigned to each node. The nodal points may be connected by thermal resistances if conduction between the nodes is to be considered. The resulting capacitance and resistance values make up a resistance-capacitance network. This network is similar to an electrical network in that the thermal capacitance is similar to the electrical capacitance, the thermal conductance is similar to the electrical conductance, the temperature of the nodes is analogous to the electrical voltage potential, and the heat flux is analogous to the electrical current.

2.2 Fuel Rod Thermal Network

The CINDA-3G[4] code used in THETA1-B considers three types of nodes -- diffusion, arithmetic, and boundary nodes. Diffusion nodes are assigned finite thermal capacitance values and, therefore, can be used to represent regions in which thermal energy is stored. Succeeding temperature levels of diffusion nodes are determined by a solution of the transient diffusion equation. Arithmetic nodes are assigned a zero volume and, therefore, a zero capacitance value, and consequently the temperature levels of these nodes are obtained from a solution of the steady state diffusion equation. Arithmetic nodes are normally used in thermal analyzer models to determine surface temperatures when the thermal response of a surface is orderly; that is, when the surface temperature does not change drastically from one time step to another. The boundary nodes are a special type of node. The temperature levels of these nodes are not determined during the network solution but are assigned prior to an iteration.

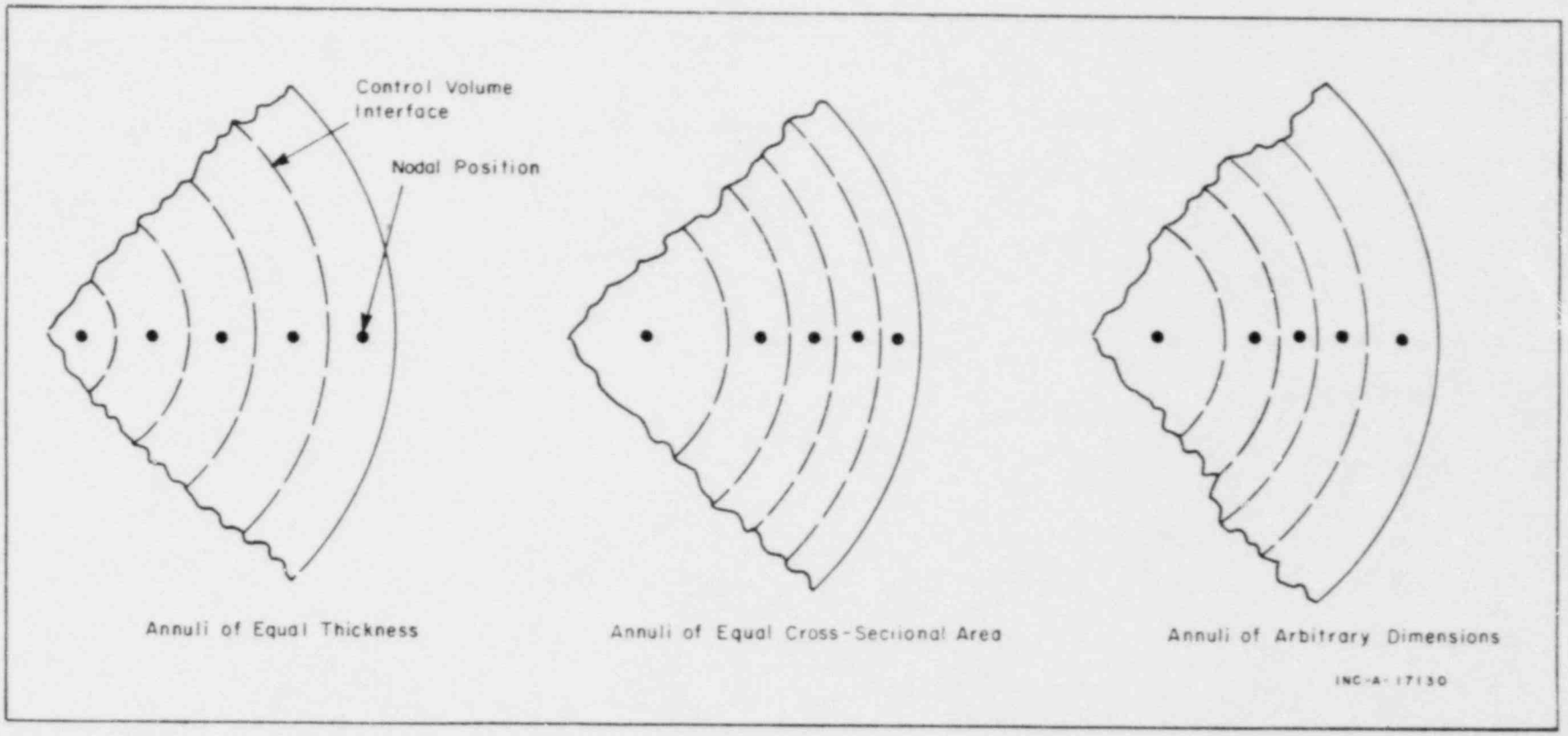

FIG. 1 FUEL RADIAL CONTROL VOLUME PATTERNS FOR FIVE RADIAL DIVISIONS.

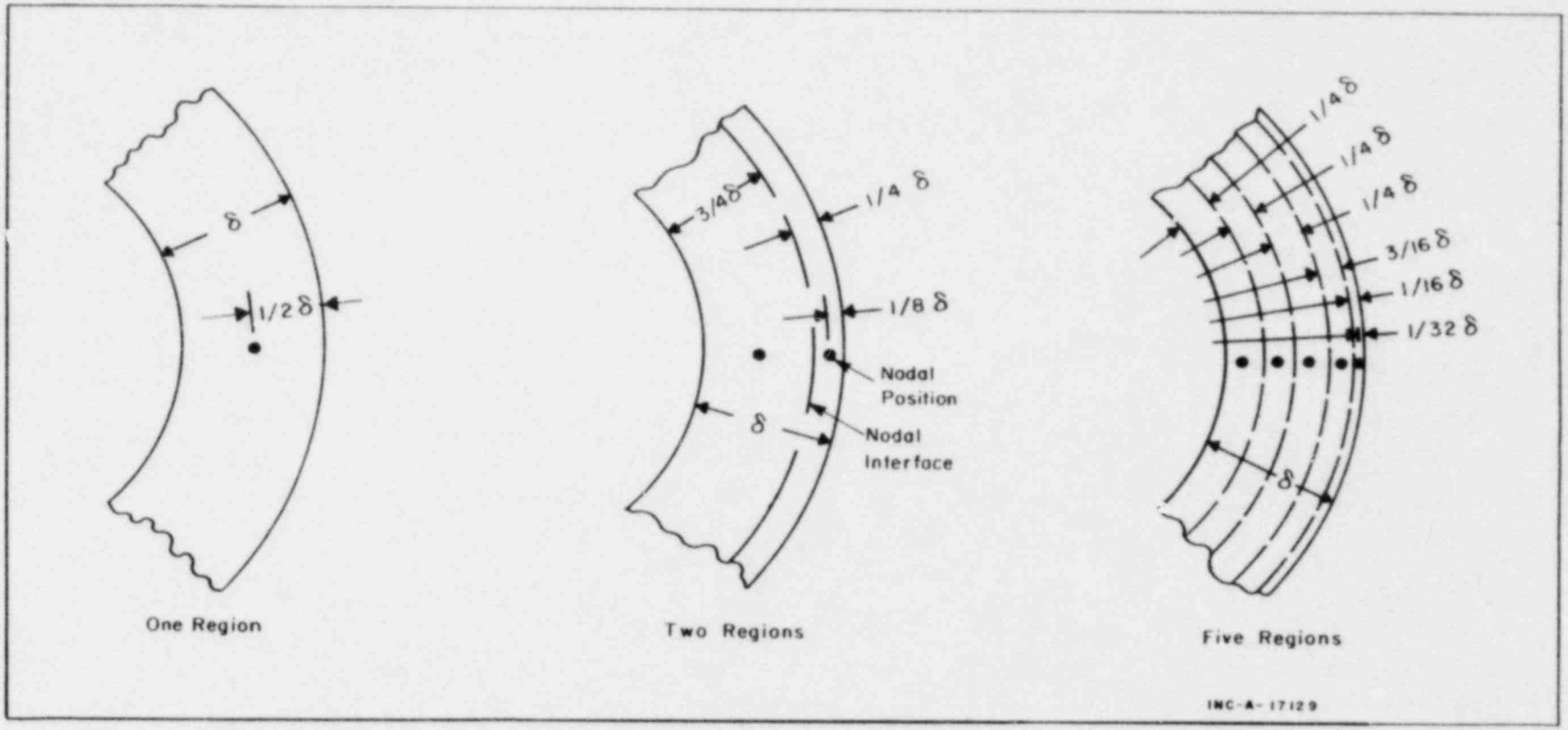

FIG. 2 CLADDING RADIAL CONTROL VOLUME PATTERNS.

In THETA1-B diffusion nodes are used to describe the fuel pellet and cladding material. All the energy is generated in the diffusion nodes. This quantity is obtained by multiplying the volumes by a power density value which is one of the supplied boundary conditions. These values are reevaluated at each new time advancement. Arithmetic nodes are used to describe the fuel pellet outer surface and the cladding inner surface, and boundary nodes are used to describe the outermost cladding region during the steady state initialization procedure.

The nodal pattern used is shown in Figure 3. The thermal conductances between nodes are represented by the standard resistance symbols. The diffusion node thermal capacitance symbols have been deleted for clarity.

The thermal capacitance terms for the diffusion nodes are evaluated in the following manner. The nodal volumes are computed and are multiplied by the material density to obtain the mass associated with each diffusion node. The thermal capacitance is obtained by multiplying the mass of each control volume by the specific heat. If the specific heat is assumed to be constant, this computation is performed only once. If a temperature dependent specific heat is used, the specific heat value is evaluated at the nodal temperature at each time step.

Thermal conductance values are obtained by multiplying the thermal conductivity by an effective area-to-length (A/ℓ) value. The (A/ℓ) term is the effective area normal to the heat flow path divided by the length between nodes. In the axial direction this term is equal to the cross-sectional control volume area divided by the axial length between nodes. In the radial direction in both the fuel pellet and the cladding the (A/ℓ) term is approximated by the quantity $2\pi k\,\ell/\ln(r_o/r_i)$ where r_o/r_i is the ratio of the larger to smaller nodal radii. As in the case for the thermal capacitance, the thermal conductance value is updated every time step if a temperature dependent thermal conductivity is used. The thermal conductivity is evaluated at the mean temperature of the two adjacent nodes of interest.

2.3 Thermal Properties

The following temperature dependent thermo-physical property data for uranium dioxide and Zircaloy-4 are recommended. This data is input as a table and may be replaced if desired.

Thermal conductivity:

Uranium dioxide[5]

$$k = \frac{1}{3600}\left\{\frac{3978.1}{T+692.61} + (6.0237 \times 10^{-12})\,(T+460)^3\right\} \qquad 77F < T < 5072F \qquad (3)$$

Zircaloy-4[45] Source: IN-1093, September 1967 by R. R. Hammer
WCAP-3269-41, May 1965 by D. B. Scott
GE-NMPO, GEMP-61, 1966

3

$$k = \frac{1}{3600}\,[8.23774 - 0.185341 \times 10^{-2}\,T + 0.213627 \times 10^{-4}\,T^2 - 0.535233 \times 10^{-7}\,T^3 + 0.727602 \times 10^{-10}\,T^4 - 0.535994 \times 10^{-13}\,T^5 + 0.215401 \times 10^{-16}\,T^6 - 0.442374 \times 10^{-20}\,T^7 + 0.362892 \times 10^{-24}\,T^8 \qquad (4)$$

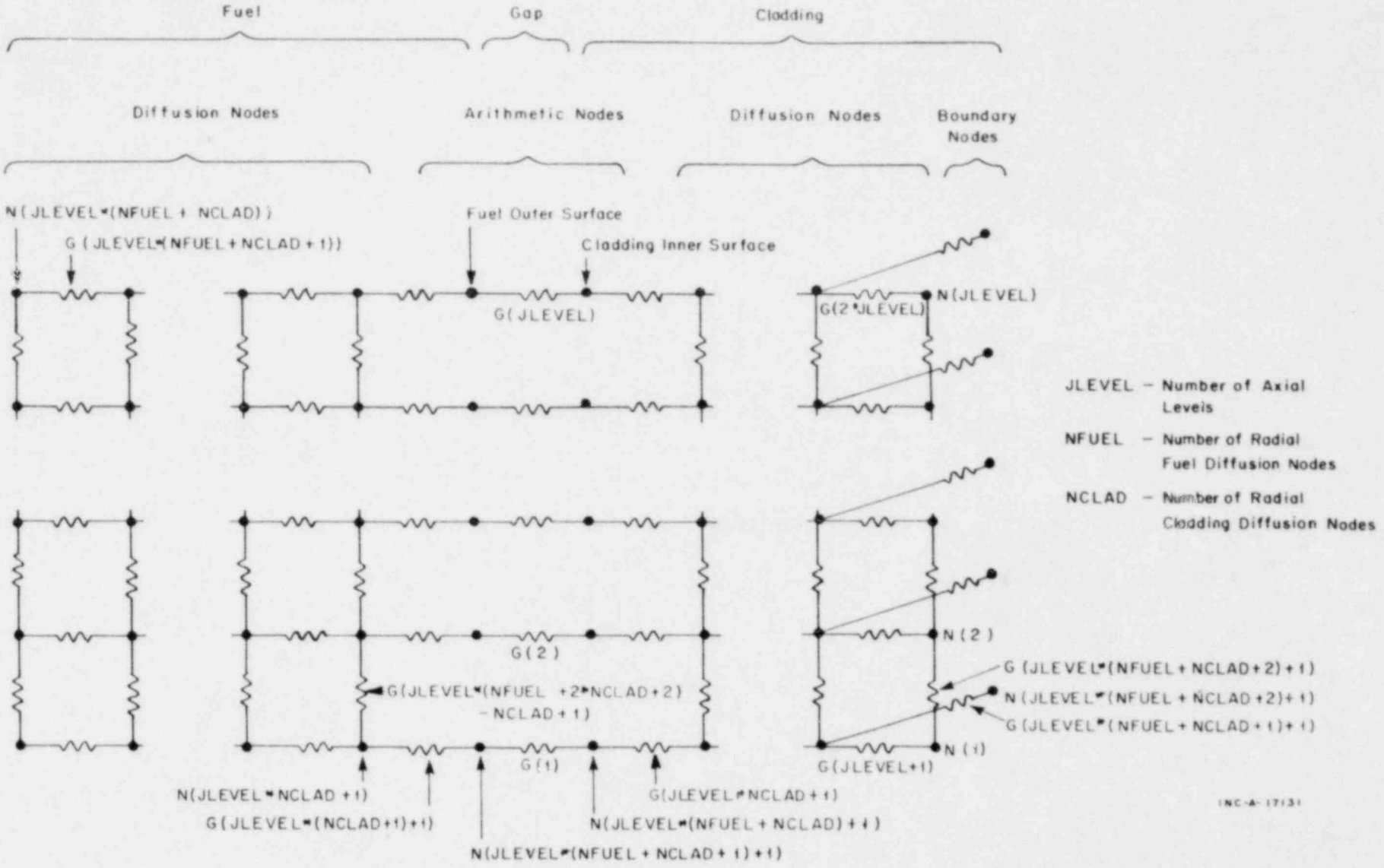

FIG. 3 GENERAL FUEL ROD NODAL NETWORK.

Specific heat:

Uranium dioxide[7]

$$C_p = 7.26 \times 10^{-2} + (3.33 \times 10^{-6})T - \frac{4.74 \times 10^3}{(T + 460)^2}$$

$$77^\circ F < T < 2240^\circ F \qquad (5)$$

$$C_p = -0.18426 + (3.3303 \times 10^{-4})\,T - (2.0447 \times 10^{-7})\,T^2 + (4.6457 \times 10^{-11})\,T^3 - (3.6289 \times 10^{-15})\,T^4$$

$$2240^\circ F < T < 5072^\circ F \qquad (6)$$

Zircaloy-4[45] (Source BMI-1803, May 1967)

$$C_p = 0.0684315 + 1.15144 \times 10^{-5}\,T$$

$$32^\circ F \leq T \leq 1062^\circ F \qquad (6a)$$

$$C_p = \text{use Figure R-3 for } T > 1062^\circ F \qquad (6b)$$

3

Figure R-3. Specific Heat of Zircaloy-4

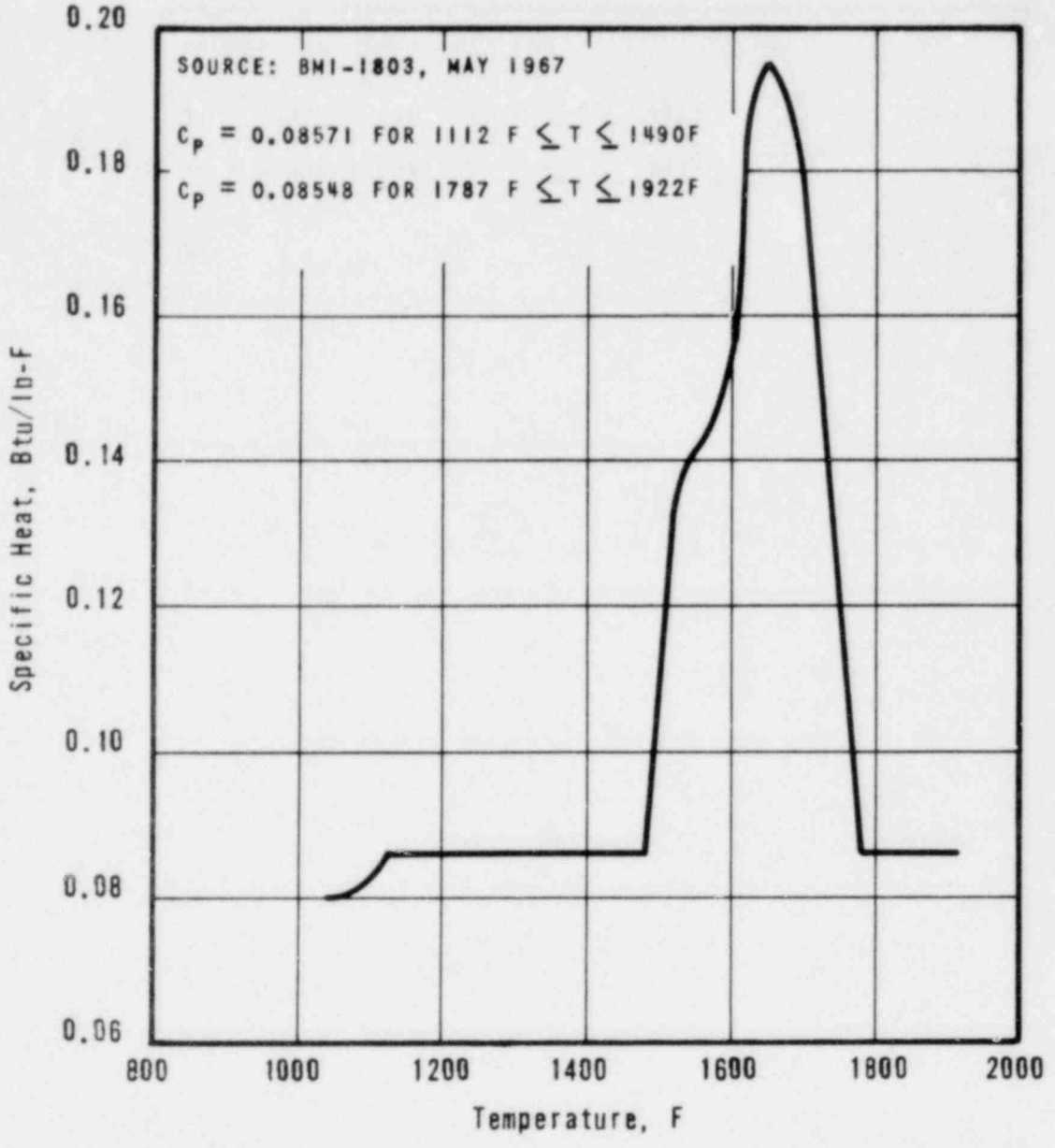

3

UO_2 conductivity correction:

The UO_2 thermal conductivity given in equation 3 is for 95% theoretical density (5% porosity). For densities other than the 95% theoretical value, the thermal conductivity of the fuel nodes is modified internally using the relation

$$k = k_{0.05}\ \text{FACTOR}$$

where k is the actual thermal conductivity, $k_{0.05}$ is the thermal conductivity of UO_2 with 95% theoretical density, and FACTOR is the conductivity correction factor. The value of FACTOR is determined using the relation

$$\text{FACTOR} = \left(\frac{1 - \text{PORS}}{0.95}\right)^3 \quad \text{for TAFY model (Loeb's method)}[34]$$

$$= \frac{1.025}{0.95}\,\frac{1 - \text{PORS}}{1 + \beta(\text{PORS})} \quad \text{TACO2 model (Maxwell Euken method)}[46]$$

where PORS = user supplied fuel porosity fraction,

$\beta = 0.5$ for PORS ≤ 0.10

$= 0.7$ for PORS > 0.10.

2.4. Gap Conductance Model

2.4.1. Prior to Cladding Failure

The gas gap heat transfer coefficien is calculated in a manner consistent with the B&W fuel rod thermal cod TAFY [34] or TACO2 [46]. The general procedure follows. 3

2.4.1.1. Reference Volumetric Temperatures

After the steady-state fuel and cladding temperature distributions have been determined, average temperatures for the fuel ($\bar{T}_{fo}$) and clad ($\bar{T}_{co}$) are calculated for each axial level. These temperatures reference the initial fuel and cladding dimensions (d_{fo} and d_{co}), which are obtained from a steady-state code (e.g., TAFY or TACO2) and input to THETA. 3

2.4.1.2. Diametral Displacement Due to Thermal Expansion

Changes in the fuel and inside cladding diameters due to thermal expansion are

$$\Delta d_{f_N} = \bar{\alpha}_f(\bar{T}_{fN} - \bar{T}_{fo})d_{fo} ,$$

$$\Delta d_{ic_N} = \bar{\alpha}_c(\bar{T}_{cN} - \bar{T}_{co})d_{c_o} ,$$

where $\bar{\alpha}_f$ and $\bar{\alpha}_c$ are the mean coefficients of thermal expansion of fuel and cladding, respectively, and are evaluated from the instantaneous values using the equation:

$$\bar{\alpha} = \frac{\int_{\bar{T}_o}^{\bar{T}_N} \alpha dt}{\bar{T}_N - \bar{T}_o} .$$ 3

Instantaneous values for the coefficients of thermal expansion, α, are as follows[7]:

$$\alpha_f = 3.72E\text{-}6 + (1.787E\text{-}9)T$$

$$32F < T < 4082F$$

$$\alpha_c = 3.10E\text{-}6 + (0.975E\text{-}9)T$$
$$32F < T < 1584F$$
$$\alpha_c = 5.4E\text{-}6$$
$$T \geq 1584F$$

2.4.1.3. Diametral Displacement Due to Differential Pressure

The time-varying fluid channel pressure is obtained from a transient thermal-hydraulics code (e.g., CRAFT2[41]) and input to THETA. Generally, only an axial segment of a fuel rod is modeled. Consequently, the time-varying internal pin pressure is also input.

The change in the fuel diameter due to the varying pin pressure is

$$\Delta d'_{f_N} = -\frac{d_{f_o}}{E_f}(1 - 2\mu_f)(P_{i_N} - P_{i_o})$$

where P_i = internal pin pressure, psi,
E = modulus of elasticity, psi,
μ = Poisson's ratio (-).

The cladding may undergo both elastic and plastic deformation at elevated temperatures.

Derivation of the elastic diametral displacement equations can be found in references 42 and 43. The inner surfaces of a thick-walled cylinder with end caps (uniform axial stress) will be displaced from the unstressed dimension by an amount

$$\Delta d_i = -\frac{d_i}{(1 - \quad E}\left[(1 + \mu)(P_e - P_i) + (1 - 2\mu)(P_e - \beta P_i)\right],$$

when subjected to an external pressure P_e and an internal pressure P_i, where $\beta = (d_i/d_o)^2$. If only the loaded diameter (d_{ic_o}) is known, the unstressed diameters may be calculated by sucessive iteration; the unstressed diameters are determined at time zero.

Since displacement prior to cladding failure is referenced from the initial compressed diameter (d_{ic_o}), the relative displacement from d_{ic_o} can be calculated as

$$\Delta d'_{ic_N} = d_{ic_N} - d_{ic_o} = \Delta d^*_{ic_N} - \Delta d^*_{ic_o}$$

where the astericks denote displacement relative to the unstressed dimension.

Changes in cladding dimensions during the period of plastic deformation preceding cladding failure are based on Hardy's [44] data, which were obtained by heating cladding maintained at fixed internal pressures to various temperatures and then venting. A typical cladding deformation curve obtained in this manner is shown in Figure 4. Three observations can be made concerning the strain within 200F of the cladding failure temperature:

1. The strain is an exponential function of temperature until very near the failure temperature.
2. At this point, the cladding expands asymptotically to its rupture diameter since its ultimate tensile strength has been exceeded.
3. The point at which this asymptotic expansion occurs is approximately 10 to 20% of the rupture strain.

The equation below is used to calculate the inside diameter of the cladding when its average temperature at a particular axial level falls within 200F of the failure temperature.

$$\Delta d'_{ic_N} = A\left(d_{ic_R} - d_{ic_o}\right) \exp\left[-B(T_R - \bar{T}_{cN})\right]$$

where

$A = 0.2$ (-),

$B = 0.0153$, F^{-1}

T_R = current failure temperature, F,

d_{ic_R} = current rupture cladding ID, in.

The current failure temperature and rupture diameter are calculated per section 2.5. When $(T_R - \bar{T}_{cN}) \leq 200F$, this diameter is compared to the diameter calculated assuming that the cladding is elastic. Since it would be unreasonable for the cladding to collapse, the maximum diameter is used. Once the swell diameter exceeds the elastic diameter, the cladding is assumed to swell plastically. The currently calculated swell diameter is compared to a previously calculated maximum, and the maximum is used. These calculations are continued to cladding failure.

Figure 4. Typical Cladding Deformation Curve

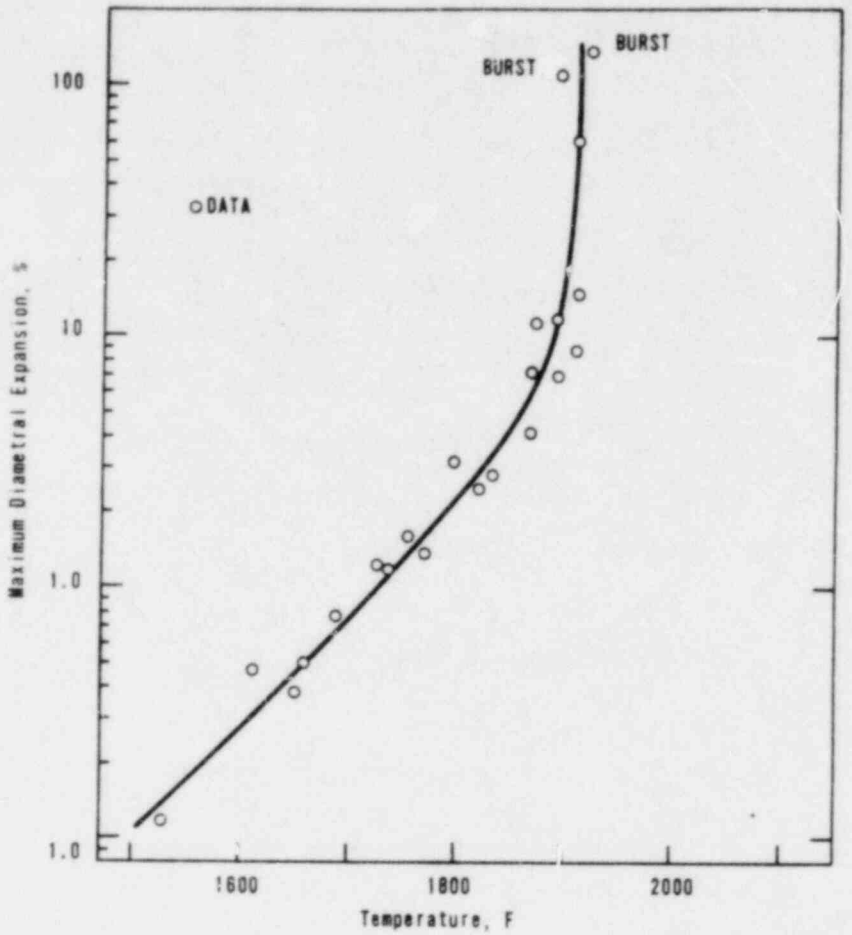

2.4.1.4. Fuel and Cladding Diameters ($t_N < t_R$)

The fuel and inside cladding diameters at t_N are

$$d_{f_N} = d_{fo} + \Delta d_{f_N} + \Delta d'_{f_N}$$

and

$$d_{ic_N} = d_{ic_o} + \Delta d_{ic_N} + \Delta d'_{ic_N}.$$

For axial levels found to swell, thermal expansion prior to cladding failure is not calculated, so that Δd_{ic_N} is set equal to zero.

2.4.1.5. Gas Gap Heat Transfer Coefficient

The heat transfer coefficient is determined using the modified Ross and Stoudte gap conductance model identical to that used in TAFY and TACO2. 3

If the fuel OD is calculated to be greater than the cladding ID, they must be in contact. For ($d_{f_N} > d_{ic_N}$), the heat transfer coefficient is calculated as

$$h = \frac{19.125\, k_m (P_f + 2845.0)}{a_o R^{1/2} H} + \frac{12k_{gas}}{c(R_1 + R_2) + (g_1 + g_2)} \quad \text{(TAFY model)}$$

$$= \frac{12k_{gas}}{c(R_1 + R_2) + (g_1 + g_2)} \quad \text{(TACO2 model)}$$ 3

where

k_m = mean conductivity of interface materials $[2k_1k_2/(k_1 + k_2)]$, Btu/s-ft-°F,

P_f = interface pressure, psi,

a_o = constant = 0.5 $cm^{1/2}$

R = mean surface roughness, $[(R_1^2 + R_2^2)/2]^{1/2}$, in.

H = Meyer hardness number for cladding, psi,

k_{gas} = thermal conductivity of gas mixture at T_{gap}, Btu/s-ft-°F,

c = contact coefficient $(2.75 - 0.000176P_f)$,

g_1+g_2 = temperature jump distances due to accomodation effect, in.

The thermal conductivity of the gas in the gap is calculated by kinetic theory.[34,46] The composition of the gas before cladding failure is helium, xenon, krypton, and air for the TAFY model and helium, xenon, krypton, oxygen, nitrogen, argon, and carbon dioxide for the TACO2 model. The mole-fraction of each gas is assumed to be constant during the transient; therefore, the thermal conductivity is dependent on gas temperature only.

The temperature jump distance is calculated by the following equations: 3

$$(g_1 + g_2) = \frac{3.94 \times 10^{-4}(T_{gap} + 460)(14.7)}{860\, P \times \sum_{i=1}^{3} \frac{k_i}{k_{gas}} \frac{\lambda_{He}}{\lambda_i}} \quad \text{(TAFY model)}$$

$$= \frac{5.448}{2.54}\left[\frac{\mu'_{gas}}{P}\left(\frac{T_{gas} + 460}{1.8M}\right)^{\frac{1}{2}}\right] \quad \text{(TACO2 model)}$$

where

T_{gap} = gap gas temperature, F,

k_i = thermal conductivity of gas i evaluated at T_{gap}, Btu/s-ft-°F,

λ_i = mean free path of gas i, cm,

μ'_{gas} = viscosity of gas mixture at T_{gap}, g/cm-s,

P = pressure of gas, psia,

M = molecular weight. 3

The contact pressure between the fuel and cladding is

$$P_f = \frac{d_{f_N} - d_{ic_N}}{\frac{1}{E_{c_N}}\left(\frac{d_{ic_N}^2}{d_{oc_N} - d_{ic_N}} + \mu_c d_{ic_N}\right) + \frac{1}{E_{f_N}}\left(d_{f_N}\right)(1 - \mu_f)}$$

If $d_{f_N} \leq d_{ic_N}$, the heat transfer coefficient is calculated as

$$h = \frac{2845 k_m (CA)(19.125)}{a_o R^{1/2} H} + \frac{12 k_{gas} (CA)}{c(R_1 + R_2) + (g_1 + g_2)}$$

$$+ \frac{12 k_{gas} (1 - CA)}{c(R_1 + R_2) + (g_1 + g_2) + (GAP_N)/[2(1 - CA)]} + h_{rad}$$

where

$$CA = F_{CA}\left\{0.1 + (0.9)(0.1)^{100\left[\left(d_{ic_N}/d_{f_N}\right) - 1\right]}\right\} \quad \text{(TAFY model)}$$

= 0.0 for TACO2 model (built in value in the code),

F_{CA} = modifying factor input as either 1 or 0 for TAFY model,

GAP_N = diametral gap size for a cracked fuel (heat transfer gap)

= uncracked gap size - initial gap closure

= $(d_{ic_N} - d_{f_N})$ for TAFY model

= $(d_{ic_N} - d_{f_N}) - (1 - f)(d_{ic_o} - d_{f_o})$ for TACO2 model, 3

f = input gap closure factor.

The radiation component is calculated as

$$h_{rad} = F_{12}\sigma\left(T_{f_N}^4 - T_{ic_N}^4\right) \Big/ \left(T_{f_N} - T_{ic}\right)$$

where T_{f_N} = fuel surface temperature, R,

T_{ic_N} = inside cladding surface temperature, R,

F_{12} = geometric emissivity factor,

$$= \frac{1}{\frac{1}{\varepsilon_f} + \left(\frac{d_{f_N}}{d_{ic_N}}\right)^2 \left(\frac{1}{\varepsilon_c} - 1\right)},$$

ε_f = emissivity of fuel,

ε_c = emissivity of cladding,

σ = Stefan-Boltzmann constant, $0.1714 \times 10^{-8}/3600$, Btu/s-ft^2-°R^4. | 3

2.4.1a. Following Cladding Failure

The gap conductances are calculated by the procedure described in section 2.4.1 prior to cladding failure. The conductances calculated at time t_N are used to calculate fuel and cladding temperatures at t_{N+1}. At each time step, the current average cladding temperature for each axial level is compared to a cladding failure temperature (section 2.5).

If rupture has occurred, the following changes are made to the gap conductance model (the following subsection headings correspond to the headings used in section 2.4.1).

2.4.1.1a. Reference Volumetric Temperatures

The volumetric average cladding temperatures at rupture reference diametral changes of the cladding.

2.4.1.2a. Diametral Displacement Due to Thermal Expansion

$$\Delta d_{f_N} = d_{fo}\bar{\alpha}_f(\bar{T}_{f_N} - \bar{T}_{fo})$$

$$\Delta d_{ic_N} = d_{ic_R}\bar{\alpha}_c(\bar{T}_{c_N} - \bar{T}_{c_R})$$

where $\bar{\alpha}_f$ and $\bar{\alpha}_c$ are evaluated as before, with $\bar{T}_{c_R}$ replacing $\bar{T}_{c_o}$ and d_{ic_R} is the cladding ID at rupture. | 3

2.4.1.3a. Diametral Displacement Due to Differential Pressure

The change in the fuel diameter due to the varying fluid channel pressure is

$$\Delta d'_{f_N} = -\frac{d_{f_o}}{E_f}(1 - 2\mu_f)(P_{e_N} - P_{i_o}) \quad |3$$

For unruptured axial levels that are elastic when rupture occurs, the strain imposed by the differential pressure is released. This calculation is performed only at rupture.

$$\Delta d'_{ic_R} = \frac{d_i}{(1 - \beta)E_c}\left[(1 + \mu_c)(P_{e_R} - P_{i_R}) + (1 - 2\mu_c)(P_{e_R} - \beta P_{i_R})\right].$$

For unruptured axial levels that have swelled, the displacement at rupture is fixed:

$$\Delta d'_{ic_R} = \Delta d'_{ic_N} \text{ @ } t_R.$$

Following rupture, it is assumed that no net force exists across the cladding.

2.4.1.4a. Fuel and Cladding Diameters ($t_N > t_R$)

The fuel and inside cladding diameters at t_N are

$$d_{f_N} = d_{f_o} + \Delta d_{f_N} + \Delta d'_{f_N}$$

and

$$d_{ic_N} = d_{ic_R} + \Delta d_{ic_N}.$$

2.4.1.5a. Gas Gap Heat Transfer Coefficient

For the ruptured axial level,

$$h = \frac{24k_{gas}}{d_{ic_N} - \quad _N} - + h_{rad}.$$

The gas is assumed to be steam, and the conductivity is calculated by the appropriate B&W subroutines.

2.5 Cladding Failure Model

The cladding failure temperature is specified by an input table where failure temperatures are tabulated as a function of cladding hoop stress. For each failure temperature, a corresponding area change ratio and cladding thickness is specified. The area change ratio is defined as the cross-sectional area of the ruptured cladding segment, A_R, divided by the design cross-sectional area, A_o. The cladding thickness, t_R, is defined as the thickness of the thinned cladding at the rupture location.

The cladding hoop stress, σ_θ, is calculated for each axial node at each time step:

$$\sigma_\theta = \frac{(P_o - P_{R_N})D_{ic}}{(D_{oc} - D_{ic})}$$

where P_o = internal pin pressure,

P_{R_N} = reactor pressure,

D_{ic} = design cladding ID,

D_{oc} = design cladding OD.

Then, the failure temperature is found by interpolation in the table. If the calculated average temperature exceeds the failure temperature, failure has occurred.

The OD of the cladding is calculated from the corresponding area change ratio:

$$d_{oc_R} = \left[\frac{4A_o}{\pi}\left(\frac{A_R}{A_o}\right)\right]^{\frac{1}{2}}.$$

The cladding ID is calculated from the corresponding rupture thickness, RTHK. If the rupture thickness is not specified, a default value is used.

$$RTHK = \frac{D_{oc}(D_{oc} - D_{ic})}{2d_{oc_R}},$$

$$d_{ic_R} = d_{oc_R} - (2 \times RTHK).$$

1

Since the dimensions of axial levels that swell may change considerably, the thicknesses of these nodes are recomputed at rupture:

$$RTHK = \frac{D_{ic}(D_{oc} - D_{ic})}{2(d_{ic_N} @ t_R)} \quad . \qquad |3$$

The length of the ruptured cladding segment is calculated by conservation of the cladding mass:

$$\ell_R = \left(\frac{D^2_{oc} - D^2_{ic}}{d^2_{oc_R} - d^2_{ic_R}}\right) \ell . \qquad |1$$

At rupture, the dimensions of the ruptured and swelled cladding nodes are used to compute new heat transfer areas and cross-sectional areas for the nodes.

3. ELECTRICAL HEATER CONDUCTION MODEL

The conduction model used to model electrically heated rods is the same as that used to model the nuclear fuel rod. The control volumes are chosen in the same manner and the nodal network is specified in the same manner.

If the heater rod is a filament-type heater, the filament is represented by one annular region. A radial power factor of one is specified for this region whereas elsewhere in the rod a radial power factor of zero is specified. A nonuniform axial power profile may also be considered. The power generation rate in the annulus representing the filament is equal to the total rod power generation rate divided by the volume of the annulus.

In a sheath heater the power is generated in the cladding material. Unity radial power factors are specified for the sheath and a zero value is specified for the insulator. The power generation rate is equal to the total rod power generation rate divided by the sheath volume.

If an electrical heater rod is being considered, temperature dependent (or constant) data for the insulator and cladding material must be supplied by the user.

4. FLUID ENERGY EQUATION MODEL

The energy balance on the fluid is described by the general energy equation for a flow situation. Several assumptions are inherent in the basic form of the energy equation that is used.

First the fluid flow problem is assumed to be one-dimensional and turbulent effects and viscous dissipation effects are neglected. Since the complete set

of conservation equations is not solved the pressure and the mass flux are assumed to be spatially constant throughout the channel. Also, thermodynamic equilibrium between the liquid and vapor phases is assumed. The two phases are allowed to travel at different velocities.

If the conservation of mass equation is combined with the conservation of energy equation and the preceding assumptions are made the energy equation may be written in the following form:

$$\rho \frac{\partial h}{\partial t} + G \frac{\partial h'}{\partial z} = \phi + \frac{\partial p}{\partial t} \tag{10}$$

The flow enthalpy h ′ is given by the expression

$$h' = h_f + x' \, h_{fg} \tag{11}$$

where the flow quality is

$$x' = \frac{\alpha \rho_g K_s}{\alpha \rho_g K_s + (1-\alpha) \rho_f} \tag{12}$$

and the slip velocity ratio is

$$K_s = \frac{\text{Vapor velocity}}{\text{Liquid velocity}} \tag{13}$$

The quantity ϕ is equal to the surface heat flux multiplied by the ratio of the wetted perimeter of the fuel rod to the cross-sectional flow area of the channel.

The slip velocity ratio may be assumed to be a constant value as specified in the input data or it may be computed internally. Currently the slip model available is a modified Bankoff correlation as proposed by Jones [8].

$$K_s = \frac{1 - \alpha}{C - \alpha + (1-C)\alpha^r} \tag{14}$$

where

$$C = 0.71 + \left(\frac{0.29}{0.32062}\right)\left(\frac{p}{10{,}000}\right)$$

and

$$r = 3.53125 - 0.1875 \left(\frac{p}{1000}\right) + 0.58594 \left(\frac{p}{1000}\right)^2.$$

If a slip velocity ratio of one is assumed the equation reduces to that for a homogeneous flow situation.

The boundary conditions required to solve the fluid energy equation are the fluid pressure, the mass flux, the enthalpy of the fluid entering the core, and the heat flux at the surface of the rod. The first three boundary conditions are obtained from a reactor system thermal-hydraulic code such as RELAP3 [2]. The pressure used is the average core pressure. The system thermal-hydraulic code solves the coupled set of conservation equations and accounts for fluid expansion effects in the core. As a result, the fluid may be flowing into or out of the core at both ends simultaneously during portions of the transient. Simultaneous flow from both ends of the core implies that a stagnation point exists at some location in the core. A conservative assumption for safety analysis purposes is that the flow rate in the core during these periods is assumed to be zero and consequently this assumption is normally made in THETA1-B. At times when the flow is predominately in one direction the mass flux and the enthalpy input are determined in the following manner. When the flow is upward through the core it is considered positive and when downward it is considered negative. The mass flux and the enthalpy at the lower plenum-core junction are input when the flow is positive and the mass flux and enthalpy at the upper plenum-core junction are input when the flow is negative. The heat flux is computed by the heat transfer routines.

The equation of state for water is required in the solution of the fluid conservation of energy equation. The steam table data used are those of Keenan and Keyes [9]. These data are presented in tabular form and a bilinear interpolation technique is used to obtain the thermodynamic properites as functions of pressure and enthalpy. The steam table data and interpolation routine used in THETA1-B was originally developed for use in the RELAP2 [10] code. The transport properties used are based on 1967 ASME Steam Table [11] data. The thermal conductivity and absolute viscosity data for saturated liquid, saturated vapor, and superheated vapor are presented in equation form and the specific heat data are presented in tabular form.

5. HEAT TRANSFER MODEL

The heat transfer model in THETA1-B assumes that the following heat transfer regimes could occur during a LOCA: forced convection in subcooled liquid or superheated steam, nucleate boiling, forced convection vaporization, transition boiling, and stable film boiling. The film boiling regime is the most important from the standpoint of the prediction of cladding temperatures during a LOCA. Consequently, several commonly accepted heat transfer correlations have been included for this regime. At the discretion of the user, alternate heat transfer correlations may be coded and added as subprograms. This feature adds versatility to the code.

The CHF prediction is also extremely important in that the time at which the CHF value is exceeded can be a crucial factor in determining the ultimate maximum cladding temperature. A number of CHF correlations have been included to allow the effect of using various correlations to be easily investigated.

The heat transfer correlations that are used in the heat transfer model are discussed in the following sections. The range of parameters and the type

of geometry used in the development of the correlations are also presented where possible.

5.1 Pre-CHF Heat Transfer Correlations

The heat transfer regimes that occur prior to the CHF condition are forced convection in subcooled liquid, nucleate boiling, and forced convection vaporization. A brief description of the conditions under which the various regimes exist follows.

During steady state operation and late in the depressurization transient during the emergency core flooding process the fluid may be in a subcooled state. During these periods the forced convection in subcooled liquid heat transfer regime will occur if the heat flux is low. If the heat flux is relatively high, subcooled nucleate boiling will exist.

If two-phase flow conditions exist and the CHF value has not been exceeded, then either a saturated nucleate boiling or forced convection vaporization regime may exist. Forced convection vaporization is also commonly referred to as annular spray heat transfer. When the void fraction is below approximately 0.8 to 0.9, the flow regime will be of a bubbly nature and nucleate boiling will exist. When the void fraction is high the postulated flow pattern will consist of a liquid film covering the rod surfaces and a core composed primarily of vapor with entrained liquid droplets; that is, an annular type flow pattern [12] will exist. The forced convection vaporization regime will exist when the flow pattern is annular in nature. Forced convection vaporization consists of two basic heat transfer mechanisms; conduction and evaporation. The nucleate boiling in the liquid covering the rod is suppressed and the heat transfer mechanism is primarily conduction through the liquid film with evaporation occurring at the liquid film-mist core interface. The heat transfer coefficient for the forced convection vaporization regime is lower than that for the nucleate boiling regime.

The heat transfer correlations used to describe the pre-CHF regimes follow. The experimental conditions for which the correlations were developed are also presented.

5.11 Forced Convection in Subcooled Liquid and Superheated Vapor.

Dittus and Boelter [13]

$$h = 0.023 \left(\frac{12\,k}{D_e}\right) (Pr)^{0.4} \left(\frac{G\,D_e}{12\,\mu}\right)^{0.8}$$

(a) Turbulent flow of water in circular tubes

$L/D > 60$

$0.7 < Pr < 100$

$Re > 10^4$

(b) Turbulent flow of steam in circular tubes [14]

Length: 36 in.

Diameter: 0.5 in.

L/D > 26

Pressure: 25 to 75 psia

Inlet temperature: 300 to 1100°F

Wall temperature: to 1800°F

Heat flux: 2400 to 31,000 Btu/ft^2-hr

5.12 Nucleate Boiling.

Jens and Lottes [15]

$$\dot{q} = \left(\frac{\Delta T_{sat} e^{p/900}}{14.7} \right)^4$$

Vertical upflow of water in round and square tubes

Length: 3 to 24.6 in.

Diameter: 0.143, 0.183, and 0.226 in.

Pressure: to 2000 psia

Mass flux: to 7.65 x 10^6 lb_m/ft^2-hr

Heat flux: to 3.5 x 10^6 Btu/hr-ft^2

Thom [16]

$$\dot{q} = \left(\frac{\Delta T_{sat} e^{p/1260}}{4.32} \right)^2$$

Vertical upflow of water

Round tube: 0.5-in. diameter, 60-in. length

Annulus: 0.7-in. ID, 0.9-in. OD, 12-in. length

Pressure: 750 to 2000 psia

Mass flux: 0.77 x 10^6 to 2.80 x 10^6 lb_m/hr-ft^2

Heat flux: to 0.5 x 10^6 Btu/ft^2-hr

5.13 Forced Convection Vaporization.

Schrock and Grossman[17]

$$h = (2.50)\ (0.023)\ \left(\frac{12\ k_f}{D_e}\right)\ (Pr_f)^{0.4}\left[\frac{G\ D_e\ (1 - x')}{12\ \mu_f}\right]^{0.8}\left(\frac{1}{\chi_{tt}}\right)^{0.75}$$

$$\frac{1}{\chi_{tt}} = \left(\frac{x'}{1 - x'}\right)^{0.9}\left(\frac{\rho_f}{\rho_g}\right)^{0.5}\left(\frac{\mu_g}{\mu_f}\right)^{0.1}$$

Water in round tubes

Diameter: 0.1162 to 0.4317 in.

Length: 15 to 40 in.

Pressure: 42 to 505 psia

Mass fluxes: 0.175×10^6 to 3.28×10^6 lb_m/ft^2-hr

Heat flux: 0.06×10^6 to 1.45×10^6 Btu/hr^2-hr

Exit quality: 0.05 to 0.57

5.2 Post-CHF Heat Transfer Correlations

After the CHF condition has occurred, transition and film boiling heat transfer regimes will exist. Several of the flow film boiling correlations that are commonly accepted are incorporated in the heat transfer model. The heat transfer mechanism during the transition from nucleate boiling to stable film boiling is less well understood and very few transition boiling correlations exist. In general, the transition boiling regime is expected to exist for a short period of time and the effect of the correlation on the long term cladding temperature is expected to be small.

The post-CHF pool boiling model was incorporated in the heat transfer model to handle the situation when stagnation occurs at some point in the core during a LOCA. This situation has been predicted by the RELAP3[2] code for a variety of break locations in typical large PWR's. Most heat transfer correlations developed for flow boiling conditions predict a zero heat flux if the flow rate is zero and consequently pool boiling correlations are required to describe the heat transfer process when the flow rate is zero. If flow stagnation does occur in the reactor core during the early portion of a LOCA, the CHF value will normally be exceeded prior to the time when the flow actually stagnates; that is, the CHF value will be exceeded as the flow is decelerating. Therefore, a pool boiling CHF correlation is not required and the pool boiling model need only cover the post-CHF part of pool boiling heat transfer.

Due to the lack of pool boiling data for water in rod bundles at high pressures the pool boiling model is founded mainly on data for geometries other than a reactor geometry and for fluids other than water. A small amount of pool boiling data exists for water at pressures near atmospheric pressure and a considerable amount of data exists for cryogenics and organic compounds

at high reduced pressure ratios. A number of stable film correlations for pool boiling for cryogenic and organic systems have appeared in the literature. The Morgan [35] pool film boiling correlation is used in THETA1-B. |3

The heat transfer correlations used to describe the post-CHF regimes and the range of parameters for which the correlations were developed are as follows:

5.21 Transition Boiling

McDonough, Milich, and King[21]

$$\dot{q} = \dot{q}_{CHF} - C(T_w - T_{w,CHF})$$

P	C
2000	0.272
1200	0.328
800	0.417

|3

Vertical upflow of water in round tubes

Diameter: 0.152 in.

Length: 12.5 in.

Mass flux: 0.2×10^6 to 1.4×10^6 lb_m/ft^2-hr

Wall temperature: $T_w < 1030°F$

Pressure: 800, 1200, and 2000 psia

5.22 Stable Film Boiling.

Dougall and Rohsenow[22]

$$h = 0.023 \left(\frac{12\ k_g}{D_e}\right) (Pr_g)^{0.4} \left[\left(\frac{\rho_g D_e}{12\ \mu_g}\right) \left(\frac{Q_g + Q_f}{A_{flow}}\right)\right]^{0.8}$$

Vertical upflow of Freon-113 in round tubes

Diameter: 0.408 and 0.108 in.

Length: 15 in.

Pressure: 2 to 9 psig

Mass flux: 3.32×10^5 to 8.18×10^5 lb_m/ft^2-hr

Heat flux: 14,400 to 41,800 Btu/ft^2-hr

Quality: up to 50%

Miropol'skiy[23]

$$h = 0.023 \left(\frac{12\ k_g}{D_e}\right) (Pr_{v,w})^{0.8} \left[\left(\frac{G\ D_e}{12\ \mu_g}\right) \left(x + \frac{\rho_g}{\rho_f}(1 - x)\right)\right]^{0.8} Y$$

$$Y = 1 - 0.1\ (1 - x)^{0.4} \left(\frac{\rho_f}{\rho_g} - 1\right)^{0.4}$$

Water flow in round tubes

Mass flux: 0.3×10^6 to 1.5×10^6 lb_m/ft^2-hr

Pressure: 580 to 3200 psia

Quality: 6 to 100%

Groeneveld[24]

$$h = 3.27 \times 10^{-3} \left(\frac{12\ k_g}{D_e}\right) (Pr_{v,w})^{1.32} \left[\left(\frac{G\ D_e}{12\ \mu_g}\right)\left(x + \frac{\rho_g}{\rho_f}(1 - x)\right)\right]^{0.901} Y^{-1.50}$$

$$Y = 1 - 0.1\ (1 - x)^{0.4} \left(\frac{\rho_f}{\rho_g} - 1\right)^{0.4}.$$

Vertical and horizontal flow of water in round tubes and annuli

Diameter: 0.06 to 1.00 in

Pressure: 500 to 3100 psia

Massflux: 0.2×10^6 to 3.0×10^6 $lb_m/hr\text{-}ft^2$

Quality: 10 to 90%

Heat flux: 35,000 to 700,000 $Btu/ft^2\text{-}hr$

Modified Dougall and Rohsenow

$$h = .023 \left(\frac{12\ k_g}{D_e}\right) (Pr_g)^{0.4} \left[\left(\frac{\rho_g\ D_e}{12\ \mu_g}\right)\left(\frac{Q_g + Q_f}{A_{flow}}\right)\right]^{0.8} \left(\frac{T_B}{T_W}\right)^{0.5}$$

5.23 Pool Film Boiling

Morgan[35]

$$h = \frac{k}{L}(.0216)\ Pr^{1/3}\left[\frac{Gr^2\ Pr^{-2/3}\left(.1212 + .1756\ \frac{h_{fg}}{c_p\ \Delta T}\right)}{\left(.1212 + .1756\ \frac{h_{fg}}{c_p\ \Delta T} + 0.0889\ Pr^{-2/3}\right)^2}\right]^{1/5}$$

$$Gr = g\left(\frac{\rho_L - \rho_v}{\rho_v}\right)L^3\ \frac{\rho_v^2}{\mu_v^2}$$

$$\Delta T = T_W - T_{sat}$$

vertical flat plate

benzene, methanol, carbon tetrachloride

5.3 CHF Heat Transfer Correlations

The CHF model in THETA1-B consists of a number of individual CHF correlations and selected combinations of these correlations. The following correlations may be used individually: Westinghouse W-3[25], General Electric[26], Macbeth[27], Barnett[28], Becker[29], Babcock & Wilcox B&W-2[30], Modified Barnett[31], and Babcock & Wilcox BWC[47]. The correlations are also combined in the following manner: 3

(1) Combination of Westinghouse W-3[25] and General Electric[26] correlations

$x \leq 0.0$	W-3
$x > 0.15$ GE	GE
$0.0 < x \leq 0.15$	Smaller of the two values predicted by the W-3 and GE correlations.

(2) Combination of Westinghouse W-3[25] and Barnett[28] correlations

$p \geq 1500$ psia	W-3
$p < 1500$ psia	Barnett

(3) Combination of Babcock & Wilcox B&W-2[30], Barnett[28], and Modified Barnett[31] correlations | 3

$p \geq 1500$ psia	B&W-2
$1500 > p > 1300$	Interpolation between B&W-2 and Barnett.
$1300 \geq p \geq 1000$	Barnett.
$1000 > p > 725$	Interpolation between Barnett and Modified Barnett
$725 \geq p$	Modified Barnett

(4) Combination of the BWC[47], Barnett[28], and Modified Barnett[31] correlations: | 3

$p \geq 1600$ psia	BWC
$1600 > p > 1300$	Interpolation between BWC and Barnett
$1300 \geq p \geq 1000$	Barnett
$1000 > p > 725$	Interpolation between Barnett and Modified Barnett
$725 \geq p$	Modified Barnett

As the mass flux approaches zero some of the CHF correlations will predict a CHF value that approaches zero. Since a zero CHF value is unreasonable a minimum value of 90,000 $\frac{\text{Btu}}{\text{ft}^2\text{-hr}}$ is set if the predicted value falls below this number. This lower limit is set in all cases including the situation in which the user adds his own choice of CHF correlation.

In the option in which the Babcock & Wilcox B&W-2 (or BWC), the Barnett, and Modified Barnett correlations are combined the CHF value is based directly on the correlations when the mass flux is above 200,000 lbm/ft^2-hr. The 200,000 lbm/ft^2-hr value is chosen as a lower limit for use of the correlations because these correlations predict the available experimental data to within ±15% or conservatively only down to this value of mass flux. Since the capability of the correlations to predict the data below a mass flux of 200,000 lbm/ft^2-hr is in doubt, the following technique is employed to approximate a CHF value for the lower mass fluxes. The correlation for the particular pressure range is evaluated at the current pressure and at a mass flux of 200,000 lbm/ft^2-hr. Then an interpolation is performed between this value and the minimum allowable CHF value of 90,000 Btu/ft^2-hr. | 3

A nonuniform flux factor is combined with the Westinghouse W-3, the Babcock & Wilcox B&W-2 and BWC CHF correlations for steady state calculations. However, since the flux factor was not developed for accelerating and decelerating flow situations it is not used during transient computations. |3

The critical heat flux correlations available in THETA1-B follow. The range of parameters and the geometry of the test apparatus used to develop the correlations are tabulated.

Westinghouse W-3 [25]

$$\dot{q}_{CHF,U} = \left(\frac{10^6}{3600}\right)\left\{(2.022 - 0.0004302\,p) + (0.1722 - 0.0000984\,p)\cdot \exp\left[(18.177 - 0.004129\,p)\,x_{CHF}\right]\right\}\cdot\left[1.157 - 0.869\,x_{CHF}\right]\cdot \left[\left((0.1484 - 1.596\,x_{CHF} + 0.1729\,x_{CHF}\,|\,x_{CHF}\,|\right)\left(\frac{3600\,G}{10^6}\right) + 1.037\right]\cdot \left[0.2664 + 0.8357\cdot\exp(-3.151\,D_e')\right]\cdot \left[0.8258 + 0.000794\,(h_f - h_{in})\right] F_s$$

where

$$F_s = 1.0 + 0.03\left(\frac{3600\,G}{10^6}\right)\left(\frac{TDC}{0.019}\right)^{0.35}$$

and TDC is an empirical mixing factor.

$$F = \frac{\dot{q}_{CHF,U}}{\dot{q}_{CHF,NU}}$$

$$F = \frac{c\int_{\ell_{incipient}}^{\ell_{CHF}} \dot{q}(z)\exp[-C(\ell_{CHF} - z)]\,dz}{\dot{q}_{local}[1 - \exp(-C\ell_{CHF,U})]}$$

and

$$C = \frac{(12)\,(0.44)\,(1 - x_{CHF})^{7.9}}{\left(\frac{3600\,G}{10^6}\right)^{1.72}}$$

Water flow in circular and rectangular tubes
Equivalent diameter: 0.20 to 0.74 in.
Length: 10 to 144 in.
Pressure: 1000 to 2300 psia
Mass flux: 1.0×10^6 to 5.0 to 10^6 lb_m/ft^2-hr
Inlet enthalpy: ≥ 400 Btu/lb_m
Quality: -0.15 to +0.15

General Electric correlation[26]

$$\dot{q}_{CHF,\ p=1000} = \left(\frac{10^6}{3600}\right)\left[0.705 + 0.237\left(\frac{3600\,G}{10^6}\right)\right] \quad x_{CHF} < x_1$$

$$= \left(\frac{10^6}{3600}\right)\left[1.634 - 0.270\left(\frac{3600\,G}{10^6}\right) - 4.71\,x_{CHF}\right] \quad x_1 < x_{CHF} < x_2$$

$$= \left(\frac{10^6}{3600}\right)\left[0.605 - 0.164\left(\frac{3600\,G}{10^6}\right) - 0.653\,x_{CHF}\right] \quad x_2 < x_{CHF}$$

$$x_1 = 0.197 - 0.108\left(\frac{3600\,G}{10^6}\right)$$

$$x_2 = 0.254 - 0.026\left(\frac{3600\,G}{10^6}\right)$$

For pressures other than 1000 psia.

$$\dot{q}_{CHF,p} = \dot{q}_{CHF,\ p=1000} + \left(\frac{440}{3600}\right)(1000-p)$$

Water flow in tubes

Equivalent diameter: 0.245 to 1.25 in.

Length: 29 to 108 in.

Pressure: 600 to 1450 psia

Mass flux: 0.4×10^6 to 6.0×10^6 lb_m/ft^2-hr

Quality: to 0.45

Macbeth[27]

$$\dot{q}_{CHF} = \left(\frac{10^6}{3600}\right)\left[\frac{A + 0.25\,D_e\left(\frac{3600\,G}{10^6}\right)(h_f - h_{in})}{B + L}\right]$$

$$A = 67.6\,D_e^{0.83}\left(\frac{3600\,G}{10^6}\right)^{0.57}$$

$$B = 47.3\,D_e^{0.57}\left(\frac{3600\,G}{10^6}\right)^{0.27}$$

Water in rod bundles

Rod diameter: 0.20 to 0.550 in.

Length: 36 to 72 in.

Pressure: 1000 psia

Mass flux: 0.18×10^6 to 4.0×10^6 lb_m/ft^2-hr

Inlet subcooling: 0 to 283 Btu/lb_m

Barnett[28]

$$\dot{q}_{CHF} = \left(\frac{10^6}{3600}\right)\left[\frac{A + B\,(h_f - h_{in})}{C + L}\right]$$

$$A = 67.45\, D_{HE}^{0.68} \left(\frac{3600\,G}{10^6}\right)^{0.192} \left|1 - 0.744 \exp\left(-6.512\, D_{HY} \left(\frac{3600\,G}{10^6}\right)\right)\right|$$

$$B = 0.2587\, D_{HE}^{1.261} \left(\frac{3600\,G}{10^6}\right)^{0.817}$$

$$C = 185.0\, D_{HY}^{1.415} \left(\frac{3600\,G}{10^6}\right)^{0.212}$$

$$D_{HY} = D_o - D_I$$

$$D_{HE} = \frac{D_o^2 - D_I^2}{D_I}$$

$$D_I = D_{rod}$$

$$D_O = \left[D_{rod}\,(D_{rod} + D_{HE}^*)\right]^{1/2}$$

$$D_{HE}^* = \frac{4\,(\text{flow area})}{\pi S\, D_{rod}}$$

$$S = \sum_{rods} \frac{\dot{q}_{rod}}{\dot{q}_{max}}$$

Water in annulus: Applied to rod bundles using "equivalent" diameters.

Equivalent diameters: $0.258 \text{ in.} < D_{HE} < 3.792 \text{ in.}$

$0.127 \text{ in.} < D_{HY} < 0.875 \text{ in.}$

Length: 24 to 108 in.

Pressure: 1000 psia

Mass flux: 0.14×10^6 to 6.20×10^6 lb_m/ft^2-hr

Inlet subcooling: 0 to 412 Btu/lb_m

Becker[29]

$$\dot{q}_{CHF} = \left(\frac{G}{4L/D_e}\right) [(h_f - h_{in}) + x_{CHF}\, h_{fg}]$$

$$x_{CHF} = 0.68\, \pi\, r_1\, x_{RD}$$

and π is the ratio of heated to wetted perimeter, r_1 is a correction factor that is a function of $\dot{q}$.

x_{RD} is the burnout steam quality in a round duct at corresponding flow conditions.

Both r_1 and x_{RD} are presented in graphical form in Reference 29.

Water in rod bundles

Rod diameter: 0.396 to 0.543 in.

Length: 23.9 to 144 in.

Pressure: 285 to 1000 psia

Mass flux: 0.059×10^6 to 1.1×10^6 lb_m/ft^2-hr

Heat flux: 0.235×10^6 to 1.0×10^6 Btu/ft^2-hr

Inlet subcooling: 5 to 430°F

Babcock and Wilcox B&W-2[30]

$$\dot{q}_{CHF} = \left\{ \frac{1.15509 - 0.40703\, D_e}{(3600)\,(12.710)\,[3.0545\,(\frac{3600\,G}{10^6})]^A} \right\} \cdot$$

$$\left\{ (0.3702 \times 10^8)\,[0.59137\,(\frac{3600\,G}{10^6})]^B - 0.15208\, x_{CHF}\, h_{fg}\,(3600\,G) \right\}$$

$$A = 0.71186 + (0.20729 \times 10^{-3})\,(p - 2000)$$

$$B = 0.8304 + (0.68479 \times 10^{-3})\,(p - 2000)$$

3

$$F = \frac{\dot{q}_{CHF,U}}{q_{CHF,NU}}$$

$$F = \frac{1.025C \int_o^{\ell_{CHF}} \dot{q}(z)\, \exp[-C(\ell_{CHF} - z)]\, dz}{\dot{q}_{local}\,[1 - \exp(-C\ell_{CHF,U})]}$$

$$C = \frac{(12)\ (0.249)\ (1 - x_{CHF})^{7.82}}{\left(\frac{3600\ G}{10^6}\right)^{0.457}}$$

Water in rod bundles

Equivalent diameter: 0.2 to 0.5 in.

Length: 72 in.

Pressure: 2000 to 2400 psia

Mass flux: 0.75×10^6 to 4.0×10^6 lb_m/ft^2-hr

Burnout quality: -0.03 to 0.20

Modified Barnett[31]

$$q = \left(\frac{10^6}{3600}\right)\left[\frac{A + B\ (h_f - h_{in})}{C + L}\right]$$

$$A = 73.71\ D_{HE}^{0.052}\ \left(\frac{3600\ G}{10^6}\right)^{0.663}\ \left(\frac{888.6}{h_{fg}}\right)\left\{1 - 0.315 \exp\left[-11.34\ D_{HY}\ \left(\frac{3600\ G}{10^6}\right)\right]\right\}$$

$$B = 0.104\ D_{HE}^{1.445}\ \left(\frac{3600\ G}{10^6}\right)^{0.691}$$

$$C = 45.55\ D_{HY}^{0.0817}\ \left(\frac{3600\ G}{10^6}\right)^{0.5866}$$

Water in rod bundles

Rod diameter: 0.395 to 0.543 in.

Length: 32.9 to 174.8 in.

Pressure: 150 to 725 psia

Mass flux: 0.03×10^6 to 1.7×10^6 lb_m/ft^2-hr

Inlet subcooling: 6 to 373 Btu/lb_m

Babcock & Wilcox BWC[47]

$$\dot{q}_{CHF} = \frac{A_5[(3600A_1G)^{A_3} + A_4(p-2000) - A_8 \chi_{CHF} h_{fg}(3600G)]}{3600[(3600A_2G)^{A_6} + A_7(P-2000)]F}$$

$$F = \frac{C \int_0^{\ell_{CHF}} \dot{q}(z) \exp[-c(\ell_{CHF} - z)]dz}{\dot{q}_{local}[1 - \exp(-c\ell_{CHF})]}$$

$$C = \frac{12 B_1(1 - \chi_{CHF})^{B_2}}{(3600G/10^6)}$$

3

Coefficient of these equations are given in the proprietary version of reference 47.

Water in bundles (17 × 17 MK-C geometry)

Length: 144 in.

Pressure: 1600 to 2400 psia

Mass flux: 1.0×10^6 to 3.5×10^6 lbm/ft^2-h

Burnout quality: -0.20 to +0.30

Equivalent diameter: 0.39 to 0.47 in.

5.3.1 CHF Heat Transfer Correlations for Low Mass Flux

The Macbeth[38] low flow correlation is used to calculate DNB fluxes at low mass fluxes. Macbeth defines the boundary dividing low and high flow correlations as shown in Figure R-2. The boundary for length to diameter ratio of 200 is internal to the code, but may be overridden by the user. |3

Macbeth Low Flow Region

$$\dot{q}_{CHF} = \left(\frac{10^6}{3600}\right) \frac{1}{158} h_{fg} \left(\frac{3600\ G}{10^6}\right)^{0.51} (1 - x)\ D_e^{-0.1}$$

Water flow in tubes
Correlation of low-velocity regime world data

The Griffith[39] countercurrent flow correlation also predicts critical heat fluxes at low mass fluxes.

$$\dot{q}_{CHF} = F(\alpha) \frac{1}{3600} \frac{\pi}{24} h_{fg} \left(\frac{1}{v_f + v_g}\right)^{0.5} [\sigma g g_o (\rho_f - \rho_g)]^{0.25} \quad |3$$

where $$F(\alpha) = 0.80 \cos\left(\frac{49\alpha + 1}{100} \pi\right) \quad |3$$

Water flow in annuli
Equivalent diameters: 0.075 to 4.98 in.
Length: 1 and 2 in.
Pressure: Atmospheric
Mass flux: 0 to 0.3 $lb_m/hr\text{-}ft^2$
Inlet subcooling: 5^oF maximum

The Macbeth low flow and Griffith countercurrent CHF correlations are used in conjunction with the previous CHF correlations in the following manner.

When the mass flux falls within the applicable range of the Macbeth low flow region (see Figure R-2), the maximum CHF value of the correlation selected from Section 5, Macbeth, and Griffith will be used. A minimum CHF value of 90,000 $Btu/hr\text{-}ft^2$ is set if the predicted value falls below this number.

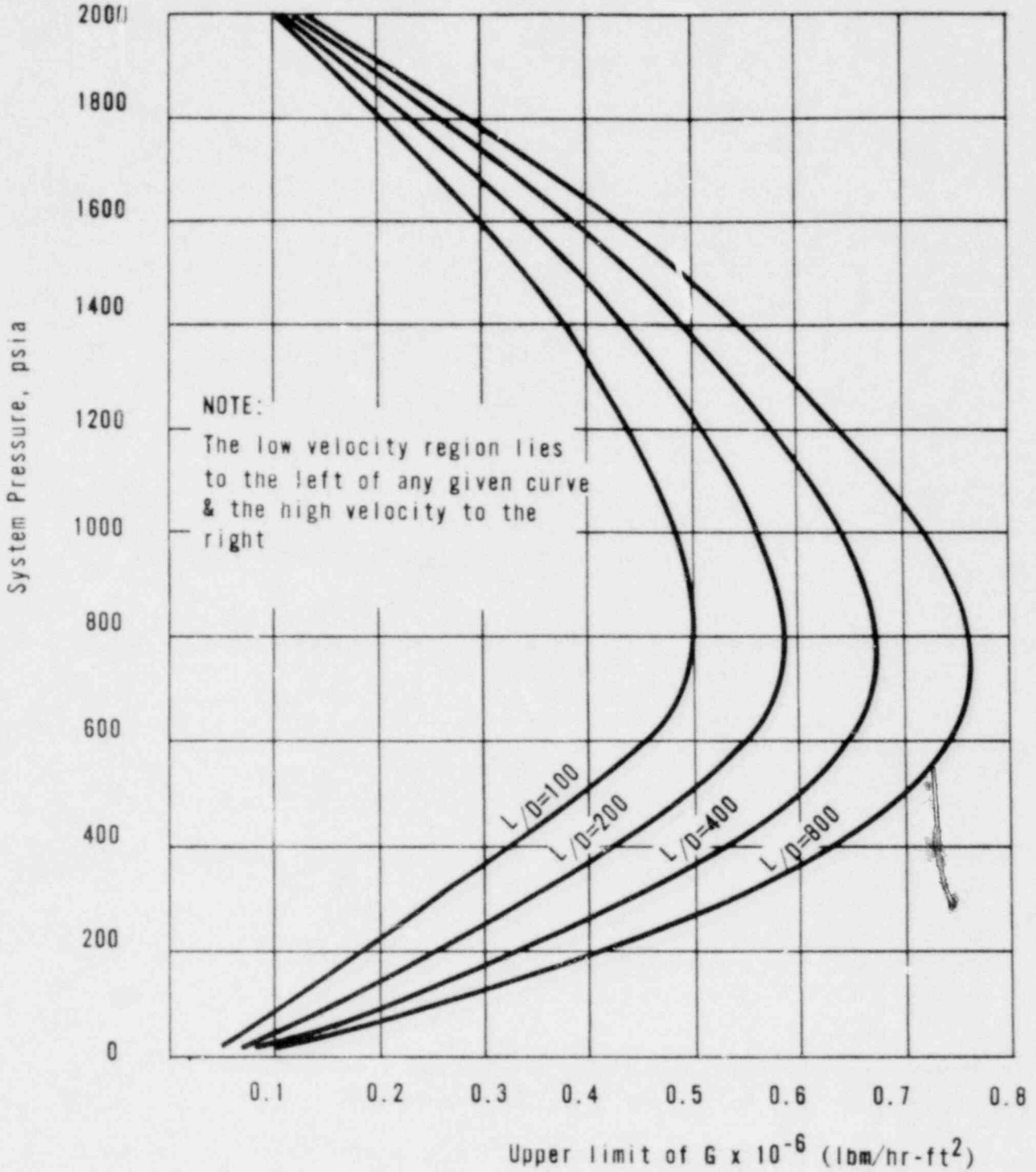

APPROX: BOUNDARY LIMITS OF THE LOW VELOCITY & HIGH VELOCITY BURNOUT REGIMES FOR ROUND TUBES

Figure R-2

5.4 Recommended Heat Transfer Correlations

The following correlations are recommended for use in analytical studies. As more accurate correlations become available they can be added to the THETA1-B heat transfer library.

(1) Forced convection -- subcooled liquid -- Dittus & Boelter[13]
Forced convection -- superheated vapor -- Dittus & Boelter

(2) Nucleate boiling -- Thom[16]

(3) Forced convection vaporization -- Shrock and Grossman[17]

(4) Transition boiling -- McDonough, Milich, King[21]

(5) Stable film boiling -- Dougall and Rohsenow[22]

(6) Pool film boiling -- Morgan[35]

(7) CHF model -- combination of Babcock and Wilcox B&W-2[30] Barnett[28], and Modified Barnett[31] correlations.

5.5. Stipulations on Heat Transfer

The following stipulations on heat transfer switching logic comply with regulations contained in the Code of Federal Regulations, Part 50, Appendix K – "ECCS Evaluation Models."

1. DNB SWITCHING – Subsequent to CHF at a particular axial node, regression on the transition boiling curve is restricted to heat fluxes (a) less than CHF for local fluid void fractions less than 80%, (b) less than the heat flux calculated by interpolation between nucleate boiling and forced convection vaporization for local void fractions between 80 and 90%, or (c) less than the heat flux calculated by forced convection vaporization for local void fractions greater than 90%. That is, transition boiling heat fluxes are restricted to values less than those calculated using pre-CHF correlations appropriate to local fluid conditions. 2

   In the event that the local transition boiling heat flux is calculated to exceed the heat flux calculated using pre-CHF correlations according to local fluid conditions, the local heat flux is determined by switching to film boiling. Thus, any return to nucleate boiling is replaced by a temporary switch to film boiling. Note that this temporary switch will not lock in a mode as described in item 3 below.

2. CLADDING SUPERHEAT SWITCHING – If the cladding superheat exceeds 300F for a particular axial node, when flow transition boiling is calculated to occur, flow film boiling will be forced. Neither flow transition boiling nor any pre-CHF boiling regime will be reapplied to this node for the remainder of blowdown, even if the cladding superheat returns to below 300F.

3. TRANSITION/POST-TRANSITION SWITCHING – If flow film boiling, pool boiling, or forced convection to superheated vapor are calculated to occur for a particular axial node, neither flow transition boiling nor any pre-CHF boiling regime will be reapplied to this node for the remainder of blowdown.

4. POOL TRANSITION BOILING has been replaced by the more conservative Morgan correlation, which extrapolates to zero heat flux at zero wall superheat.

6. METAL-WATER REACTION

When Zircaloy is raised to an elevated temperature in a steam atmosphere, an exothermic reaction will occur. The heat of reaction of this process is 2800 Btu/lbm. As the cladding temperatures rises, the reaction becomes more violent. The metal-water reaction is calculated by the Baker-Just [32] parabolic rate equation.

$$\frac{dr}{dt} = -\frac{3.0204 \times 10^{-4} K_{mw}}{\rho_m^2 (R - r)} \exp\left[\frac{\Delta E}{\mathring{R} (T + 460)}\right]$$

$$= -\frac{0.0611}{R - r} \exp\left(-\frac{41,200}{T + 460}\right) \quad \text{for Zircaloy cladding} \qquad 3$$

where r is measured in inches, ρ_m is the cladding density (lbm/ft^3) for the metal-water reaction, K_{mw} is the reaction rate constant (mg^2/cm^4-s), ΔE is activation energy (cal/mole), and $\mathring{R}$ is the universal gas constant (=1.1039 cal/mole/R). The metal-water reaction occurs on the outside of the cladding and on the inside surface of the failed cladding node after failure occurs. The reaction may or may not be steam-limited at user option.

The oxide thinning model thins the oxide layer as the cladding expands. Since the metal-water reaction rate increases inversely with the thickness of the oxide layer, the model conservatively calculates the exothermic heat release. Thinning is calculated by conservation of the oxide mass.

$$\Delta X^N = \frac{d^{N-1} \ell^{N-1}}{d^N \ell^N} \Delta X^{N-1}$$

where ΔX^{N-1} = oxide thickness at t^{N-1} (after reaction),

ΔX^N = oxide thickness at t^N (before reaction),

d = oxide diameter,

ℓ = node length.

The metal-water reaction computation may be included or omitted as desired by the user. The effect of the metal-water reaction may be determined by comparing results both with and without the option. 3

7. REFLOODING HEAT TRANSFER COEFFICIENTS

Reflood heat transfer coefficients versus real time are input by the user. As an option, heat transfer coefficient are generated internally using the FLECHT[37] correlations.

7.1 FLECHT Correlations

Figure R-1 represents a typical reflood time history for a given flood rate from the beginning of the reflood period until the time the cladding is quenched by the axially advancing "quench front".

For empirical correlation purposes, FLECHT heat transfer behavior at a given elevation is divided into three periods as shown. Period I corresponds to steam and dispersed flow regimes. Period III corresponds to a stable film boiling regime which extends to the time at which the clad surface begins to rewet (quench). Period II spans the time interval between dispersed flow and the establishment of a vapor film.

The FLECHT correlations are used to determine heat transfer coefficients at the axial level where the peak power density occurs. The highest cladding temperature at the end of adiabatic heat up is used.

7.2 Variable Flooding Rate

The FLECHT correlations were developed for a constant flooding rate. Most likely, the flooding rate will vary with time. The following procedure is used to juxtapose the heat transfer histories for step changes in flooding rates.

For a step change, a time history is computed for the new flooding velocity. An equivalent flooding time, t_{EQ} is computed such that the total water injected into the core is the same.

$$V_{m+1}\, t_{EQ} = \sum_{i=1}^{m} V_i \, (t_{END_i} - t_{o_i})$$

where

V_i = ith flooding velocity

V_{m+1} = new flooding velocity, in/sec

t_{o_i} = start of flooding velocity V_i, sec

t_{END_i} = end of flooding velocity V_i, sec.

The heat transfer coefficient for the new flooding rate is evaluated at t_{EQ} using the FLECHT correlations. Then it is compared to the previously calculated heat transfer coefficient, $h(t_{END_m})$.

If $h(t_{EQ} < h(t_{END_m})$, a conservative, discontinuous drop to the new curve is made. If $h(t_{EQ}) > h(t_{END_m})$, the new flooding history is run back until the heat transfer coefficients are equal. The subsequent time history is computed using the FLECHT correlation for the new flooding velocity.

This procedure is continued for successive flooding rates until the end of reflood.

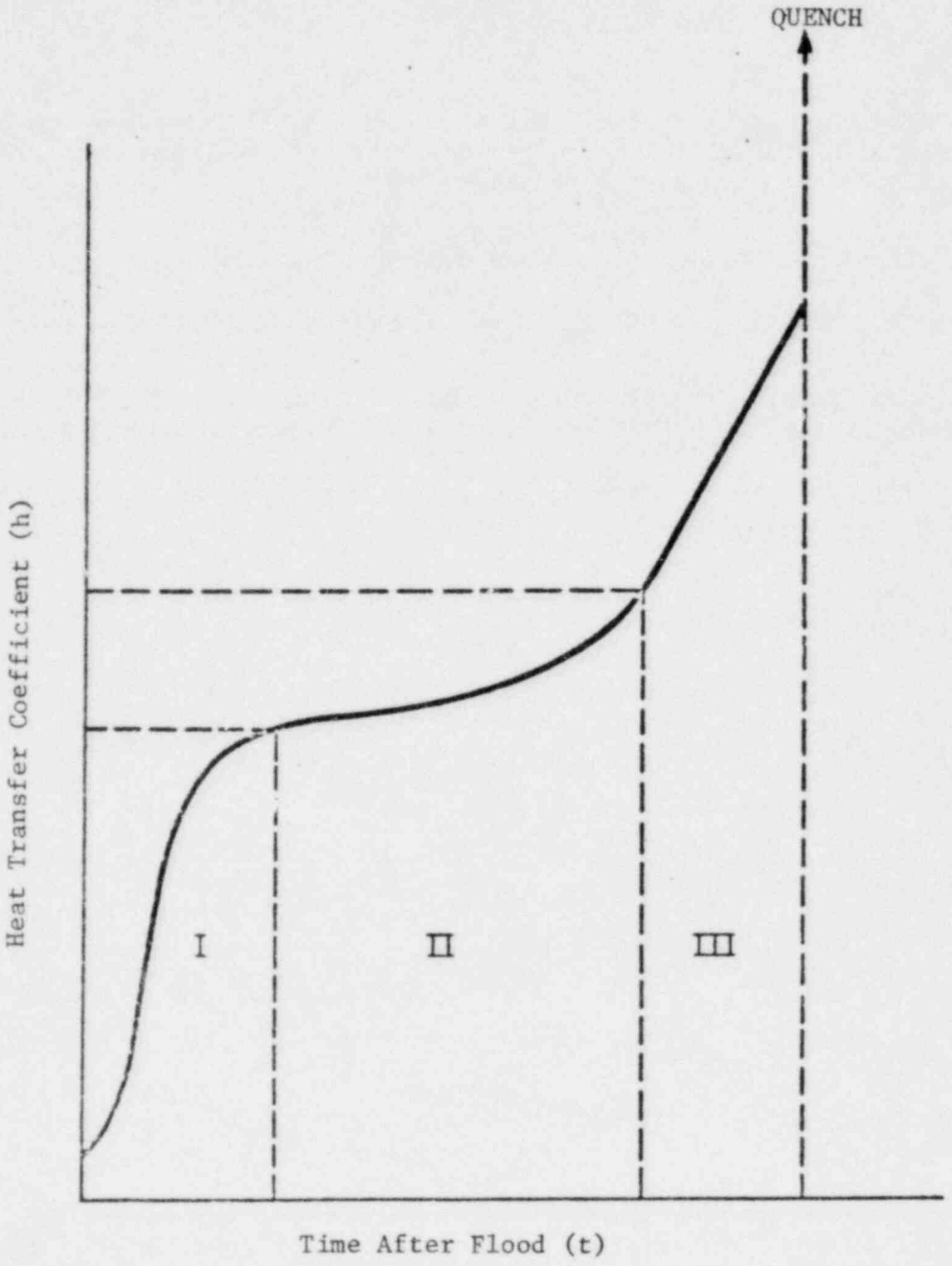

Fig. R-1 TYPICAL REFLOOD TIME HISTORY

III. SOLUTION PROCEDURE

The basic solution sequence used is described in this section. First the overall logic involved in the steady state and transient phases is outlined. Then the procedures used to solve the fuel rod conduction equation and the fluid energy equation, and to determine the appropriate heat transfer regime and heat flux are discussed.

1. GENERAL SOLUTION SEQUENCE

For a steady state solution the energy equations in the fuel rod and in the fluid channel are solved in an iterative manner to obtain the temperature distribution in the fuel rod and the fluid enthalpy distribution in the fluid channel. First the localized surface heat flux is estimated on the basis of the power generation rate in the fuel rod. Axial conduction effects are neglected in the initial estimate of the heat flux. An initial enthalpy distribution in the fluid channel is computed on the basis of the fluid pressure, inlet enthalpy, mass flux, and estimated surface heat flux. Once the fluid state and the surface heat flux have been estimated the heat transfer model is used to determine whether a subcooled forced convection or a nucleate boiling heat transfer regime is present. Then the cladding surface temperature can be estimated. Then by using the estimated surface temperature and the power generation rate, and by assuming constant thermal conductivity in the fuel pellet and cladding, an initial temperature distribution in the fuel rod can be estimated. Once these initial estimates have been made an iterative technique is used to obtain the final thermodynamic state of the system. The final solution is attained when prescribed convergence criteria are met.

The solution sequence during a transient is outlined briefly. The solutions of the fuel rod energy equation and the fluid energy equation are solved independently during any one time step advancement. The uncoupling is accomplished by assuming that the heat flux is constant over a given time step. The thermodynamic states of both the rod and fluid are used to determine the heat flux at the end of the time step.

First, the temperature distribution in the fuel rod is updated by using the old heat flux value and the average power generation rate over the time step interval. Two basic solution techniques may be used to solve the RC network. If the explicit technique is used, the desired time step size, which is an input value, is automatically reduced if it exceeds a maximum allowable time step size as determined by a stability analysis. A check is also made to determine whether the nodal temperatures have changed more than a specified amount and, if they have, the temperature distribution is recomputed using a reduced time step size. These checks are again made to assure that the maximum allowable change criteria are satisfied. If the implicit scheme is chosen the same procedure is used except that a stability analysis places no limit on the time step size.

The next step in the solution sequence is the solution of the fluid energy equation. As for the fuel rod, the old value of the heat flux is used as a boundary

condition during the time advancement. New values of pressure, mass flux, and inlet enthalpy are obtained from the data that are supplied by the user and the new fluid state is determined. By using the new cladding surface temperature, the new mass flux, and the new thermodynamic state of the fluid, the heat transfer model is used to determine the new value of the heat flux and the heat transfer regime. When the heat flux has been determined, the computations for the next time step advancement are begun.

2. FUEL ROD CONDUCTION EQUATION SOLUTION PROCEDURE

If the diffusion equation is differenced in the usual manner, a set of equations can be written involving the thermal capacitance and the thermal conductance terms. The resulting set of algebraic equations is solved by the CINDA-3G [4] code in either an explicit or implicit manner. In the explicit solution scheme the conduction equation is forward-differenced in time. The desired temperatures are now expressed entirely in terms of known quantities and can be determined directly. The alternate technique utilized is an implicit method commonly known as the Crank-Nicholson technique. In this scheme the conduction equation is mid-differenced in time such that both old and new values appear in the spatial derivative term. The new temperature values cannot be written explicitly in terms of old known values. Consequently an iterative technique must be used to solve this set of coupled algebraic equations. The differencing procedures for both the explicit and implicit schemes are presented in Appendix A.

No restrictions are placed on the allowable time step that may be used in the implicit scheme except that the time steps must be small enough to allow any rapid changes in the boundary conditions to be picked up. Even though relatively large time steps may be used in the implicit scheme the solution time is long due to the iterative procedure that is required to solve the equations. A stability analysis shows that a fairly restrictive criterion is placed on the allowable time step that may be used in the explicit scheme. Even with this time step size restriction the explicit solution technique is relatively fast due to the simplicity of the method. For this reason the explicit technique is normally used.

The network that is solved by the CINDA-3G code was shown in Figure 3. The outermost nodes in the cladding are represented by two different types of nodes that are used during different portions of the solution. During the steady state initialization these regions are represented by the designated boundary nodes; the diffusion nodes N(1) through N(JLEVEL) are disconnected from the network. During the transient, the boundary nodes are disconnected and the diffusion nodes N(1) through N(JLEVEL) are used to determine the transient response of the node representing the cladding surface. Boundary nodes were used during the initialization because the use of such nodes simplified the basic solution logic.

3. FLUID ENERGY EQUATION SOLUTION PROCEDURE

During the development of the THETA1-B code, several numerical differencing techniques were developed to solve the conservation of energy equation for the fluid. Various techniques were tried until experience indicated that a stable and accurate technique had been developed. The first technique used was an explicit scheme. In its original form it was unstable. An alteration to the scheme gave it conditional stability but the resulting accuracy was poor. In the author's opinion the poor accuracy primarily is due to the very small size of the ratio

$$(\Delta t^n / Dz_j)$$

where

Δt^n = n^{th} time step ($n > 0$)

Dz_j = length of j^{th} control volume ($j = 1, \ldots, JLEVEL$)

In many practical applications this ratio will be very small. A more detailed description of this technique is presented in Appendix B.

A six-point implicit technique was then developed. This technique was not restricted by a time step criterion but accuracy was poor. The inaccuracy again was probably due in part to the very small size of $(\Delta t^n / Dz_j)$. Experience with this technique has shown that if an error is introduced in the solution early in the transient it tends to remain throughout the solution. Appendix C provides more information concerning the details of the numerical analysis method.

A third technique is presented in Appendix D. This method consists of a combination of a two-step Lax Wendroff technique [33] and a complementary technique, both of which are explicit. The original two-step Lax-Wendroff technique is conditionally stable only for time step sizes less than some limiting value. To overcome this shortcoming, a complementary scheme was developed by using the same approach as was used in the development of the original technique. The resulting method is also conditionally stable but for time step sizes larger than the limiting value for the original two-step method. The combination of the two techniques provides an overall scheme that is unconditionally stable with the exception of several situations that occur rarely, if at all. These situations are discussed in Appendix D. Although this technique proved to be better than either the explicit or implicit techniques, the small size of $(\Delta t^n / Dz_j)$ also had a damaging effect on the accuracy of this method. As a result, not only did inaccuracies arise in the transient solution but also, once introduced, they tended to remain throughout the rest of the transient, as discussed in Appendix D. All three of the techniques described handled rapid changes in the boundary conditions with difficulty.

The most recent numerical scheme developed is based on a method of characteristics technique. The details of the numerical analysis are presented in Appendix E. This method has proved to be stable and accurate for all cases checked to date. Apparently the accuracy and stability of this scheme are less sensitive to the small size of $(\Delta t^n / Dz_j)$ than the other schemes. This numerical scheme is recommended and is being used in current analyses.

4. HEAT TRANSFER MODEL SOLUTION PROCEDURE

The manner in which the heat transfer regimes are linked together is described in this section. Since the steady state initialization and the transient portions of the solution are handled differently, the logic involved in each situation is outlined separately.

Only the subcooled forced convection and the nucleate boiling regimes are assumed to exist during the steady state initialization process. This assumption is reasonable in that present day nuclear reactors are operated at conditions such that the possibility of the CHF value being exceeded is small.

The surface heat flux at each axial level is first estimated on the basis of the localized power generation rate. During this computation axial conduction effects are neglected. The subcooled forced convection correlation is solved in an inverse manner to obtain the wall temperature that would be required to sustain the estimated heat flux in the forced convection regime. The first estimate of the local fluid state, the estimated local heat flux, and the flow rate are used in this computation. Similarly, by assuming a nuclear boiling regime, the wall temperature required to sustain the estimated heat flux is determined. Once the wall temperatures for the two heat transfer regimes are estimated, the correct heat transfer regime is determined in the following mannner. A typical flow boiling curve is shown in Figure 5. The solid line represents the map of physically possible heat fluxes and the dashed lines represent extensions of the analytical correlations. Only the subcooled forced convection and nucleate boiling regimes are considered in the following discussion. At a given heat flux the correct heat flux regime is that one which predicts the lower wall temperature.

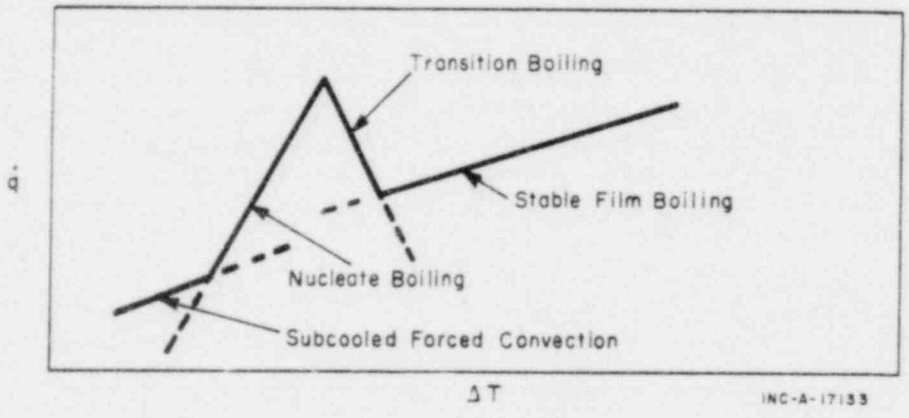

FIG. 5 FLOW BOILING CURVE.

The cladding temperature as estimated in this manner is used along with the power generation rate in the rod to determine the temperature distribution in the rod. During this computation axial conduction effects are included. The inclusion of axial conduction will result in a local surface heat flux distribution which is slightly different than the first estimate. This heat flux profile is used to obtain a new estimate of the local thermodynamic state of the coolant. Then the same method as previously described is used to obtain a

new estimate for the cladding temperature. This iterative procedure is continued until a convergence criterion is met.

Once the correct steady state heat flux distribution and the localized heat transfer regimes have been determined, a check is made to determine whether the CHF value has been exceeded. If forced convection exists at some axial level, no CHF value is computed. However, if the nucleate boiling regime is present, a CHF value is computed and is compared with the local heat flux value. If the local CHF value has been exceeded a message is printed and if a transient solution was to have been made the job is terminated.

In general, the heat transfer model links the solutions of the energy equations for the fuel rod and coolant channel at the end of each time step during the transient. At this time in the transient computation the instantaneous thermodynamic state of both the fuel rod and the fluid have been determined and the coolant flow rate has been given as a boundary condition. This information is used to determine the local heat transfer regime and the local heat flux.

The heat transfer model used in the transient solution is set up to systematically progress through the heat transfer regimes that make up the boiling heat transfer process. A check is first made to determine whether either the subcooled liquid or the superheated steam forced convection regime is present. If both the cladding temperature and the fluid temperature are above the saturated value corresponding to the current pressure, then forced convection to superheated steam exists. If the cladding temperature is below the saturation temperature and the fluid temperature is less than or equal to the saturation temperature the subcooled forced convection regime is present.

If the cladding temperature is above the saturation temperature and the fluid is subcooled then the possibility exists that either the subcooled forced convection or the nucleate boiling regime could be present. For this situation the cladding surface temperature, the thermodynamic state of the fluid, and the coolant flow rate are used to compute the heat fluxes for both the subcooled forced convection and nucleate boiling regimes. By referring to the flow boiling curve sketched in Figure 5 and by considering only subcooled forced convection and nucleate boiling for a given temperature difference the heat transfer regime which will exist will be observed to be that for which the heat flux is higher.

When the fluid is saturated and the cladding temperature is above the saturation level, the assumption is made that either of two pre-CHF heat transfer regimes could exist depending on whether a bubbly type flow regime or an annular type flow regime exists. When the void fraction is below about 0.8 to 0.9 a bubbly type or slug flow regime will most likely exist whereas above this value the flow regime changes to an annular flow or mist flow regime [12].

If either the nucleate boiling or forced convection vaporization regime has been established tentatively, a check is made to determine whether the predicted heat flux, which is based on the current difference between the wall and fluid temperatures, could actually exist. A CHF value is predicted based on the current mass flux and local thermodynamic fluid state. If the heat flux

predicted by one of the pre-CHF correlations is larger than the estimated CHF value then a post-CHF regime must exist.

The appropriate post-CHF regime is determined in the following manner. On the basis of the current cladding surface temperature and fluid saturation temperature, heat transfer rates are predicted by using both the transition and film boiling regime correlations. The correct heat flux and heat transfer regime are determined by selecting the larger of the two computed values.

The heat transfer model described in previous paragraphs is used in all cases in which the magnitude of the mass flux (flow may be in either direction through the core) is larger than 200,000 lbm/ft^2-h. Below this value of mass flux post-CHF heat transfer values are based on both pool boiling and flow boiling correlations. First the flow boiling heat transfer rate is determined by computing both transition and film boiling heat fluxes and choosing the larger value. Next, the pool boiling heat flux is computed. The flow and pool boiling heat fluxes are then compared and the larger value is chosen. The value of the mass flux at which the pool boiling check is begun was arbitrarily chosen to be a relatively large value because flow boiling is expected to be predominant above this level.

If the cladding superheat exceeds 300F for a particular axial node, when flow transition boiling is calculated to occur, flow film boiling will be forced. Neither flow transition boiling nor any pre-CHF boiling regime will be re-applied to this node for the remainder of blowdown, even if the cladding superheat returns to below 300F.

Subsequent to CHF at a particular axial node, regression on the transition boiling curve is restricted to heat fluxes (1) less than CHF for local fluid void fractions less than 80%, (2) less than the heat flux calculated by interpolation between nucleate boiling and forced convection vaporization for local void fractions between 80 and 90%, or (3) less than the heat flux calculated by forced convection vaporization for local void fractions greater than 90%. That is, transition boiling heat fluxes are restricted to values less than those calculated using pre-CHF correlations appropriate to local fluid conditions. 2

In the event that the local transition boiling heat flux is calculated to exceed the heat flux calculated using pre-CHF correlations according to local fluid conditions, the local heat flux is determined by switching to film boiling. Thus, any return to nucleate boiling is replaced by a temporary switch to film boiling.

IV. MODELING TECHNIQUES

The accuracy of the computations obtained with THETA1-B depends upon the number of regions used in the model of the fuel rod and the fluid channel. As more nodes are used the accuracy of the results increases but the computational time also increases. When an analysis is performed with a computer code, minimizing the cost of the computer runs while maintaining sufficient accuracy to give meaningful results is desirable. Therefore sensitivity analyses were performed to determine the number of radial and axial nodes required in the THETA1-B model to provide accurate results.

Since a thermal network technique is used in the solution of the fuel rod conduction equation in THETA1-B some error will exist if a finite number of radial nodes is used to describe the fuel rod. Therefore, a sensitivity analysis was performed to determine the number of radial nodes required in the THETA1-B fuel rod model to provide a reasonably accurate temperature distribution during both steady state and transient situations.

To determine how accurate the thermal network conduction model is the network results are compared with an analytical solution. The actual conduction problem being solved in THETA1-B consists of several concentric regions each having different temperature dependent thermophysical properties. The boundary conditions at the rod surface vary quite rapidly and depend upon the particular problem being solved. An analytical solution to a problem of this nature is not possible. Therefore, a simplified situation was assumed to allow an analytical solution for comparison purposes.

The following hypothetical problem was considered. An infinite cylinder has constant thermophysical properties approximating those of UO_2. The initial temperature profile is assumed to be parabolic and the surface and center-line temperatures are 0 and 3000°F, respectively. Then the surface temperature is assumed to be maintained at 0°F for some given time and no internal power is generated.

The initial parabolic temperature distribution with a center-line-to-surface temperature difference of 3000°F is typical of the temperature profile in a fuel pellet at the hot spot of an operating reactor. The boundary conditions assumed in the test problem are such that the temperature will change more rapidly than in a fuel pellet during a typical LOCA situation. Therefore, if the network solution can accurately describe the temperature profile in the test case it also is expected to do an adequate job of describing the less severe transient situation in a fuel pellet during a LOCA analysis.

The analytical solution of the sample problem is

$$T(r,t) = \frac{4\,T(o,t)}{R^2} \sum_{n=1}^{\infty} \left(\frac{1}{\alpha_n^2}\right) \frac{J_2(R\alpha_n)}{J_1^2(R\alpha_n)} J_o(r\alpha_n)\, e^{-\left(\frac{kt}{\rho C_p}\alpha_n^2\right)}$$

where Ra_n are the eigenvalues of

$$J_o(Ra_n) = 0.$$

The results are shown in Figure 6 as the solid curves.

The results of the thermal network solutions using 2, 6, 10, and 18 radial nodes are also presented in Figure 6. The network solutions were obtained with the CINDA-3G[4] thermal analyzer code. The modeling techniques used were identical to those used in THETA1-B.

The comparison of the network solutions with the analytical solution shows that the exact solution is approached as the number of nodes in the network is increased. The network solution approaches the exact solution from above as the number of nodes is increased. Appendix F proves that the network solution will approach the exact solution from above for steady state conditions. The analysis approach used in Appendix F could also be extended to the transient situation and would show that the transient temperature distribution predicted by the network approach would approach the exact solution from above.

Most of the THETA1-B transient analyses are performed using six radial nodes in the fuel pellet. The results of this sensitivity study indicate that six radial nodes are adequate to provide a reasonably accurate temperature distribution in the fuel rod during typical accident conditions.

An axial sensitivity analysis was also performed to determine the number of axial levels required to predict the steady state minimum CHF ratio accurately. A hot rod in a typical current generation pressurized water reactor was considered. The rod was divided into 7, 11, and 19 axial levels and a symmetrical axial power factor curve was assumed. The minimum CHF ratios computed for the 7, 11, and 19 axial level cases were 2.08, 2.02, and 2.01, respectively. The minimum CHF ratio was accurately predicted by the 11-axial-level model. The CHF location was more accurately predicted by the 19-axial-level model because smaller control volume lengths were used. For this particular example the 11-axial-level model predicts the minimum CHF ratio accurately. However, for situations in which the axial power factor is considerably different, the number of axial levels required to accurately predict the minimum CHF ratio may be different.

An axial sensitivity analysis was not performed for transient situations. However, since the maximum temperature obtained at the cladding hot spot during a LOCA depends upon the local power factor, a general recommendation may be made that a sufficient number of axial levels be considered to adequately represent the local power factor at the hot spot.

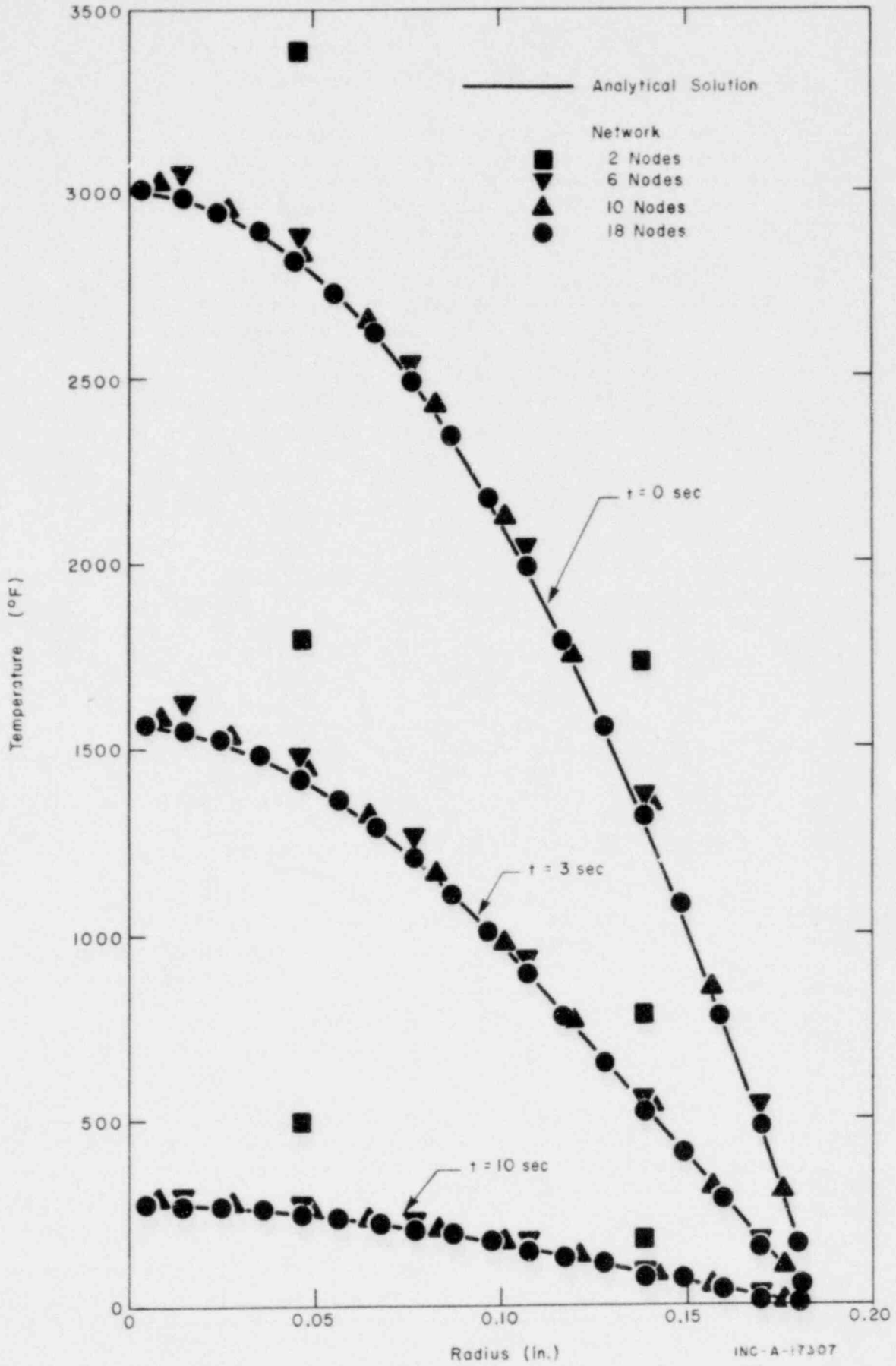

FIG. 6 RADIAL SENSITIVITY ANALYSIS.

V. TYPICAL ANALYTICAL RESULT

The results of a sample problem are presented and analyzed in this section. THETA1-B was used to determine the temperature response of the hot spot in a typical current generation pressurized water reactor during a postulated loss-of-coolant accident. The accident condition assumed was an offset shear rupture of an inlet pipe.

Since the THETA1-B code considers only the fuel rod and an associated fluid channel, the boundary conditions at the channel entrance must be obtained from a code such as RELAP3[2] which solves the conservation of mass, momentum, and energy equations for the complete reactor primary system. The data to be used as boundary conditions must be chosen with care. Very early in a depressurization the fluid pressure and flow rate may fluctuate violently due to the subcooled wave phenomena occurring during this time. The data input to THETA1-B should follow these oscillations fairly accuately. The CHF condition may occur during this time period and since the CHF phenomena are dependent on the fluid conditions they should be input as accurately as possible.

Since THETA1-B solves only the fluid energy equation and not the coupled set of conservation equations for the fluid, several simplifying assumptions are required. The pressure and mass flux are assumed to be uniform throughout the channel at any instant in time. The average core pressure as computed by RELAP3 was used as the pressure in the fluid channel. The mass flux boundary condition was obtained in the following manner. Since RELAP3 solves the coupled set of conservation equations it accounts for fluid expansion effects in the core. As a result, the fluid may be flowing into or out of the core at both ends simultaneously during portions of the transient. Such simultaneous flow implies that a stagnation point exists at some location in the core. A conservative assumption for safety analysis purposes, that is, one that will result in a cladding temperature that is higher than would actually occur, is that the flow rate in the core during these periods is assumed to be zero. At times when the flow is predominately in one direction the mass flux and enthalpy are determined in the following manner. When the flow is upward through the core it is considered to be positive and when the flow is downward it is considered to be negative. The mass flux and the enthalpy at the lower plenum-core junction are input when the flow is positive and the mass flux and enthalpy at the upper plenum-core junction are input when the flow is negative. The pressure, mass flux, and inlet enthalpy histories used during this analysis are shown in Figure 7.

The power generation rate in the fuel rod is also a required boundary condition. This quantity was obtained from the reactor kinetics model in the RELAP3 code. The power generation rate drops very rapidly to a level approximately 7% of the normal operating power and then decreases slightly during the remainder of the transient.

Through use of the boundary conditions obtained from the reactor system code, the detailed thermal response of the fuel rod and the fluid channel are computed. The predicted cladding hot spot and corresponding fuel pellet centerline temperature response during the depressurization transient are shown

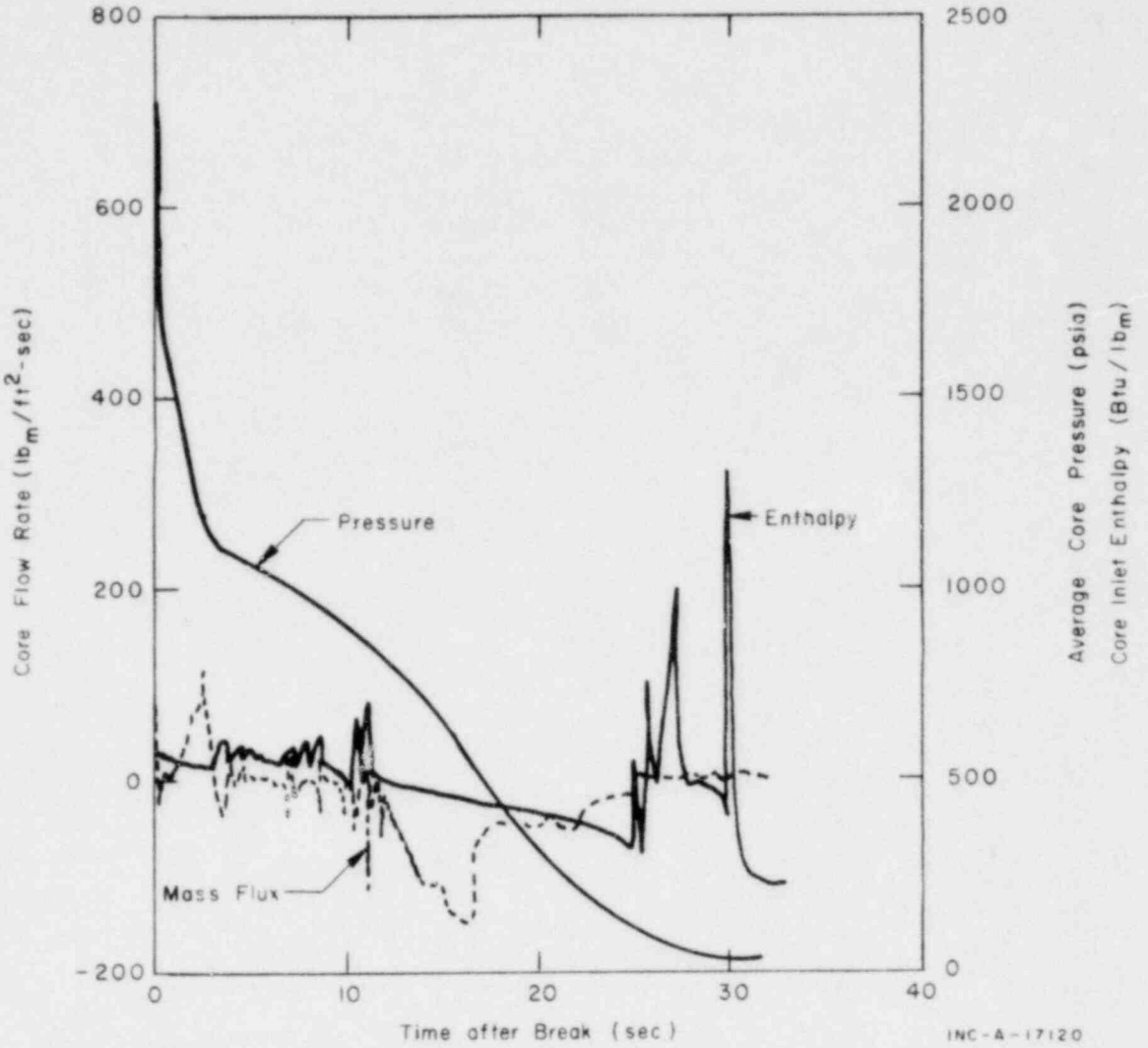

FIG. 7 TYPICAL INPUT QUANTITIES.

in Figure 8. The fluid temperature and the heat transfer coefficient at the rod-fluid interface are also presented in Figure 8.

The critical heat flux has been exceeded very early in the transient (approximately 30 msec) and a large decrease in heat transfer coefficient occurs at the rod surface. The flow rate remains essentially zero from 0.03 to 0.85 sec. Some flow fluctuations occur during this time period but their duration is small. During this period the heat transfer alternates between flow film boiling and pool film boiling regimes. The heat transfer coefficient for film boiling during this period is low compared to the pre-CHF nucleate boiling coefficient.

Due to the low thermal inertia of the cladding and the decreased heat transfer coefficient at the cladding surface the cladding temperature rises rapidly to a level that is approximately equal to that of the fuel pellet surface, but a large temperature gradient still exists in the fuel pellet. During the remainder of the transient the cladding surface temperature response is controlled by the redistribution of sensible energy in the fuel rod, the decay heating in the rod, and the film boiling mechanism at the cladding-fluid interface.

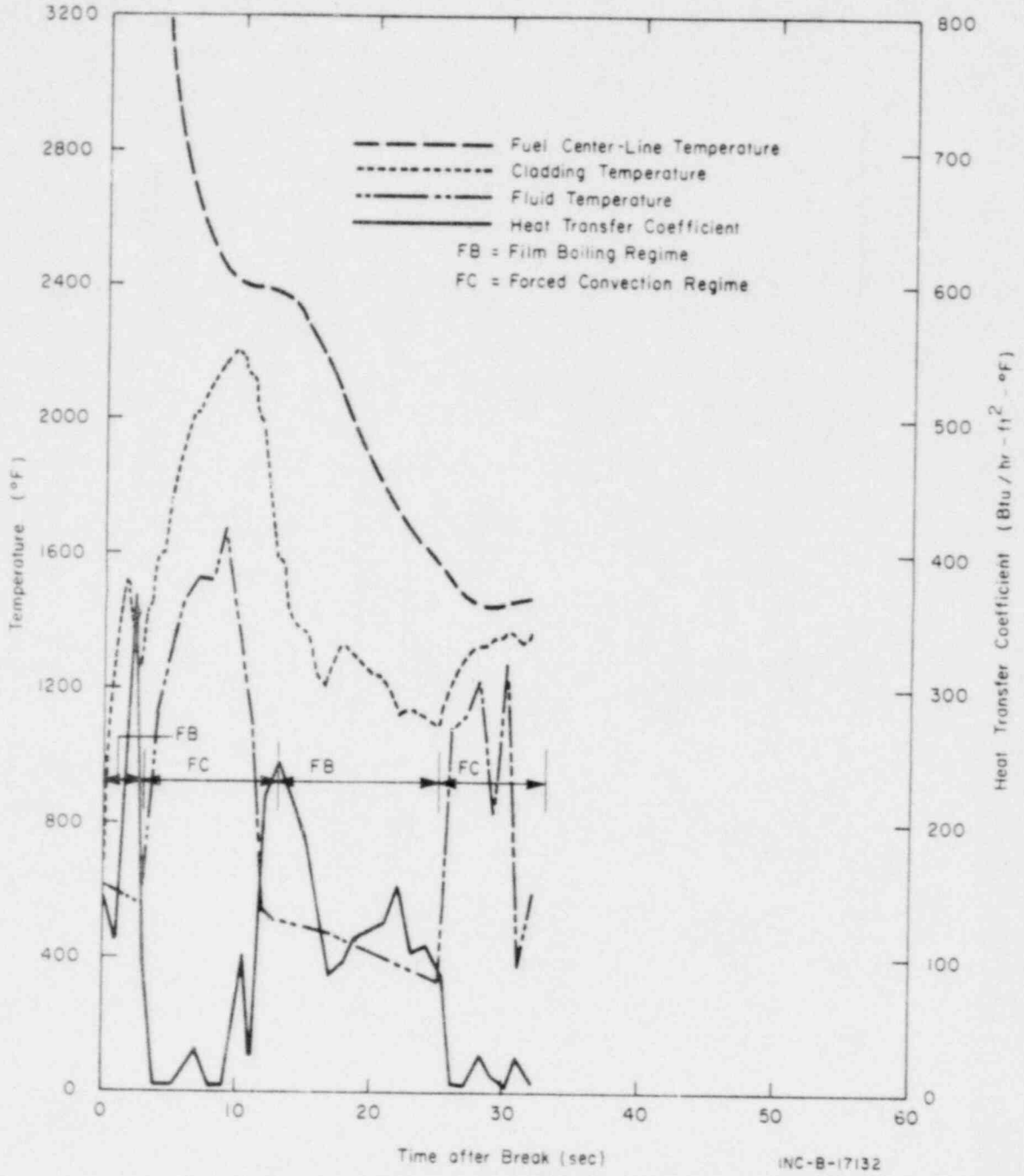

FIG. 8 TYPICAL FUEL ROD AND COOLANT THERMAL RESPONSE.

Between 0.85 and 2.5 sec the flow through the core increases and causes an increase in the flow film boiling coefficient. Eventually the heat flux at the cladding surface is increased to a level that causes the cladding temperature to decrease. From 2.5 to 3.0 sec the core flow rate decreases and the cladding temperature again rises. Between 3.0 and 6.5 sec the flow through the core is zero except for very small flow pulses. During this time period the coolant adjacent to the hot spot is in a superheated state. The surface heat flux is very low and the cladding temperature rises as energy is redistributed in the fuel pellet. The flat spot in the temperature profile is caused by a phase change in

the Zircaloy cladding material. At approximately 6.5 sec flow through the core begins to fluctuate sufficiently to reduce the rate of temperature rise of the cladding. This flow behavior continues until a maximum cladding temperature of 2200°F is reached between 9.5 and 10 sec.

Shortly after 10 sec the flow begins to fluctuate more violently and eventually an increasing negative flow rate is established. The increasing negative flow rate results in an increasing forced convection heat transfer coefficient and the cladding temperature drops significantly. At about 12 sec two-phase flow is established in the channel and a flow film boiling heat transfer mechanism exists. From this time until 25 sec the magnitude of the flow rate is sufficiently high to maintain a relatively high flow film boiling coefficient. The heat transfer coefficient is sensitive to changes in flow rate. Consequently as the flow rate increases the magnitude of the time rate of change of the cladding temperature increases and, as the flow rate decreases, the magnitude of the rate of change of the cladding temperature decreases. After 25 sec the flow reduces to a very small positive flow rate and forced convection in superheated steam occurs. The very low heat transfer coefficient results in an increasing cladding temperature.

At approximately 30 sec the temperature redistribution in the fuel pellet is complete. The combination of a low heat transfer coefficient and the decay heat power level results in an increasing fuel rod energy level as can be seen in Figure 8.

A. Plot Capability

The ability to plot has been added to THETA. The user may now select on option any or all of the following plots:

1. The inside surface cladding temperature.
2. The cladding volume – average temperature.
3. The cladding outermost diffusion node temperature.
4. The fuel volume – average temperature.
5. The gap heat transfer coefficient. 3
6. The coolant temperature.
7. The coolant heat transfer coefficient for specified axial nodes.
8. The mass flux at the entrance to the core.

The actual plotting is done by a separate program CCPLOT[36] to be run at the end of the THETA run.

VI. REFERENCES

1. H. D. Curet, J. A. Dearien, J. R. Larson, C. W. Solbrig, L. J. Ybarrondo, Loss-of-Coolant Accident Analysis Program, IN-1382 (June 1970).

2. W. H. Rettig, G. A. Jayne, K. V. Moore, C. E. Slater, M. L. Uptmor, RELAP3 -- A Computer Program for Reactor Blowdown Analysis, IN-1321 (June 1970).

3. J. Dugone, D. E. Solberg, D. H. Walker, LOFT Integral Test Program, IDO-17258K (April 1969).

4. J. D. Gaski, Chrysler Improved Numerical Differencing Analyzer for 3rd Generation Computers, Chrysler Corporation Technical Note TN-AP-67-287 (October 1967).

5. S. Y. Ogawa, E. A. Lees, M. F. Lyons, Power Reactor High Performance UO_2 Program Fuel Desigr Summary and Program Status, GEAP-5591 (January 1968). | 3

6. Y. S. Touloukian (ed.), Thermophysical Properties of High-Temperature Solid Materials, Volume 2, Part II, New York: MacMillan (1967).

7. H. C. Brassfield, J. F. White, L. Sjodahl, J. T. Bittel, Recommended Property and Reaction Kinetics Data for Use in Evaluating a Light-Water-Cooled Reactor Loss-of-Coolant Incident Involving Zircaloy-4 or 304-SS-Clad UO_2, GEMP-482 (April 1968).

8. A. B. Jones, Hydrodynamic Stability of a Boiling Channel, KAPL-2170 (1961).

9. J. H. Keenan, F. G. Keyes, Thermodynamic Properties of Steam, New York: Wiley & Sons, Inc. (1936).

10. K. V. Moore, W. H. Rettig, RELAP2 -- A Digital Program for Reactor Blowdown and Power Excursion Analysis, IDO-17263 (March 1968).

11. C. A. Meyer et al, 1967 ASME Steam Tables -- Thermodynamic and Transport Properties of Steam, New York: The American Society of Mechanical Engineers (1967).

12. A. E. Bergles, "Two-Phase Flow Structure Observations for High Pressure Water in a Rod Bundle", pp 47-55 of Two-Phase Flow and Heat Transfer in Rod Bundles, Symposium presented at the Winter Annual meeting of Mechanical Engineers, Los Angeles, California (November 1969).

13. M. Jakob, Heat Transfer Vol. I, New York: Wiley & Sons (1957).

14. P. S. Larsen, H. A. Lord, Convective and Radiative Heat Transfer to Superheated Steam in Uniformly and Nonuniformly Heated Tubes, ORA Project 08742-1-F, University of Michigan (February 1969).

15. W. H. Jens, P. A. Lottes, Analysis of Heat Transfer, Burnout, Pressure Drop, and Density Data for High-Pressure Water, ANL-4627 (1951).

16. J.R.S. Thom, et al., "Boiling in Subcooled Water During Flow Up Heated Tubes or Annuli," Proc. Inst. Mech. Engrs., Vol. 180, Part 3C (1966), pp 226-246.

17. V.E. Schrock, L.M. Grossman, Forced Convection Boiling Studies, Final Report on Forced Convection Vaporization Project, TID-14632 (1959).

20. P.A. Edwards, J.D. Obertelli, Burnout and Pressure Drop Data on 37-Rod Clusters in High Pressure Water, AEEW-R488 (1966).

21. J.B. McDonough, W. Milich, E.C. King, Partial Film Boiling with Water at 2000 psig in a Round Vertical Tube, MSA Research Corp, Technical Report 62 (1958) (NP-6976).

22. R.S. Dougall, W.M. Rohsenow, Film-Boiling on the Inside of Vertical Tubes with Upward Flow of the Fluid at Low Qualities, MIT-TR-9079-26 (1963).

23. Z.L. Miropol'skiy, "Heat Transfer in Film-Boiling of a Steam-Water Mixture in Steam Generating Tubes," Teploenergetika, Vol. 10, No. 5 (1963) pp 49-53 (AEC-tr-6252).

24. D.C. Groeneveld, An Investigation of Heat Transfer in the Liquid Deficient Regime, AECL-3281 (Rev. December 1968; Revised August 1969).

25. L.S. Tong, "Critical Heat Fluxes in Rod Bundles", pp 31-46 of Two-Phase Flow and Heat Transfer in Rod Bundles, Symposium presented at the Winter Annual meeting of the American Society of Mechanical Engineers, Los Angeles, California, November 1969.

26. E. Janssen, S. Levy, Burnout Limit Curves for Boiling Water Reactors, APED-3892 (1962).

27. R.V. MacBeth, Burn-Out Analysis: Part 5 – Examination of Published World Data for Rod Bundles, AEEW-R 358 (1964).

28. P.G. Barnett, A Correlation of Burnout Data for Uniformly Heated Annuli and Its Use for Predicting Burnout in Uniformly Heated Rod Bundles, AEEW-R 463 (1966).

29. K.M. Becker, A Burnout Correlation for Flow of Boiling Water in Vertical Rod Bundles, AE-276 (1967).

30. J.S. Gellerstedt, et al., "Correlation of Critical Heat Flux in a Bundle Cooled by Pressurized Water", pp 63-71 of Two-Phase Flow and Heat Transfer in Rod Bundles Symposium, Symposium presented at the Winter Annual meeting of the American Society of Mechanical Engineers, Los Angeles, California (November 1969).

31. E.D. Hughes, A Correlation of Rod Bundle Critical Heat Flux for Water in the Pressure Range 150 to 725 psia, IN-1412 (July 1970).

32. L. Baker, Jr., L.C. Just, Studies of Metal-Water Reactions at High Temperatures. III. Experimental and Theoretical Studies of the Zirconium-Water Reaction, ANL-6548 (May 1962).

33. R.D. Richtmyer and K.W. Morton, Difference Methods for Initial-Value Problems, 2nd Ed. InSci., John Wiley & Sons, New York (1967).

34. C.D. Morgan and H.S. Kao, TAFY — Fuel Pin Temperature and Gas Pressure Analysis BAW-10044, April 1972.

35. C.D. Morgan, A Study of Film Boiling From Vertical Surfaces, Ph.D. Dissertation, Lehigh University (1965).

36. P.W. Daggett, CCPLOT — Utility Plotting Program, NPGD-TM-213, April 1973.

37. F.F. Cadek, et al., PWR FLECHT — Full-Length, Emergency Cooling Heat Transfer, WCAP-7665 (1971).

38. R.V. Macbeth, Burnout Analysis, AEEW-267 (1963).

39. C.T. Avedisian, Critical Heat Flux in Countercurrent Flow, MS Thesis, Massachusetts Institute of Technology (1974).

40. Critical Heat Flux Limits for CNSG Conditions, BAW-1405, Babcock & Wilcox (1973).

41. R.A. Hedrick, J.J. Cudlin, and R.C. Flotz, CRAFT2 — Fortran Program for Digital Simulation of a Multinode Reactor Plant, BAW-10092, Rev 2, Babcock & Wilcox, April 1975.

42. W. Flügge, Handbook of Engineering Mechanics, McGraw-Hill, New York (1962).

43. S.P. Timoshenko and J.N. Goodier, Theory of Elasticity, 3rd Ed., McGraw-Hill, New York (1970).

44. D.G. Hardy, High-Temperature Rupture Behavior of Zircaloy Tubing, CONF-730304 USAEC/TIC, Water-Reactor Safety, March 1973.

45. Nuclear Materials Standards, Manual 2A1-N, Babcock & Wilcox, June 1980.

46. Y.H. Hsii, et al., TACO2 — Fuel Pin Performance Analysis, BAW-10141P, Babcock & Wilcox, January 1979. 3

47. R.H. Wilson, et al., BWC Correlation of Critical Heat Flux in 17×17 Geometry Rod Bundles, BAW-10143P, Babcock & Wilcox, January 1980.

APPENDIX A

NUMERICAL SOLUTION OF FUEL ROD CONDUCTION EQUATION

APPENDIX A

NUMERICAL SOLUTION OF FUEL ROD CONDUCTION EQUATION

The CINDA-3G[A-1] thermal analyzer code can be used to solve most problems that can be described by the diffusion equation. Fourier's conduction equation

$$\rho c_p \frac{\partial T}{\partial t} = k \nabla^2 T + q''' \qquad \text{(A-1)}$$

is an equation of this type and is used to describe the conduction processes in the fuel rod.

The thermal analyzer concept utilizes a lumped parameter approach to solve the conduction equation. First the region to be considered is divided into a number of finite sized elements. Then a resistance-capitance network is used to represent the region. Each subregion is represented by a node in the network. The nodes are located at the geometric center of the control volumes. The capacitance values represent the thermal capacitance of each volume and the resistors represent the thermal resistance to the flow of thermal energy between adjacent nodes.

The conduction equation, which is solved numerically, is differenced and written in a form that is similar to that describing an electrical RC network. Then the resulting set of algebraic equations are solved for the nodal temperature values.

To illustrate the numerical differencing techniques employed in CINDA-3G the one-dimensional diffusion equation written in rectangular cartesian coordinates is considered:

$$\rho c_p \frac{\partial T}{\partial t} = k \frac{\partial^2 T}{\partial z^2} + q''' \qquad \text{(A-2)}$$

The spatial net in the z-direction is sketched in Figure A-1.

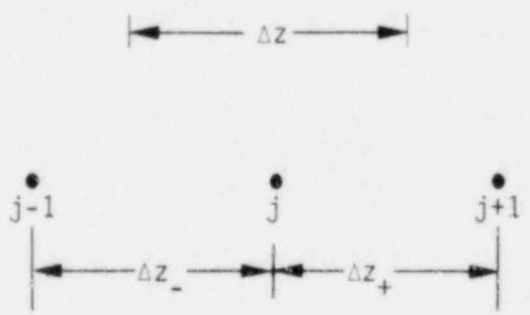

FIG. A-1 CONDUCTION MESH.

The quantity Δz represents the linear dimension of the j^{th} control volume. The quantities Δz_- and Δz_+ represent the physical distances between the three adjacent nodal locations. In the following development, subscripts will refer to spatial location and superscripts denote positions in the time dimension.

The temporal derivative is approximated by

$$\frac{\partial T}{\partial t} \approx \frac{T_{j+1}^{n} - T_{j}^{n}}{\Delta t^{n}} \qquad \text{(A-3)}$$

where Δt^{n} is the time step size. The spatial derivative

$$\frac{\partial^2 T}{\partial z^2} \approx \left(\frac{1}{\Delta z}\right) \left[\frac{T_{j+1}^{n} - T_{j}^{n}}{\Delta z_{+}} + \frac{T_{j-1}^{n} - T_{j}^{n}}{\Delta z_{-}}\right] \qquad \text{(A-4)}$$

may be approximated in terms of the nodal temperatures at the old time. The volume associated with node "j_z" is $A\Delta z$ where A is the cross-sectional area of the node perpendicular to the z-axis. Equations (A-2), (A-3), and (A-4) are combined and the resulting equation is multiplied by the volume $A\Delta z$ to obtain:

$$(\rho c_p V)_{j}^{n} \left(\frac{T_{j}^{n+1} - T_{j}^{n}}{\Delta t^{n}}\right) = \left(\frac{kA}{\Delta z}\right)_{+}^{n} (T_{j+1}^{n} - T_{j}^{n}) + \left(\frac{kA}{\Delta z}\right)_{-} (T_{j-1}^{n} - T_{j}^{n}) + Q_{j}^{n} \qquad \text{(A-5)}$$

The source term Q_j^n is equal to $V_j q'''^n$ where q'''^n is the generation per unit volume. The capacitance and conductance quantities are given by

$$C_{j}^{n} = (\rho c_p V)_{j}^{n} \qquad \text{(A-6)}$$

and

$$G_{j_{(\pm)}}^{n} = \left(\frac{kA}{\Delta z}\right)_{(\pm)}^{n} \qquad \text{(A-7)}$$

The specific heat and thermal conductivity of both the fuel pellet and cladding are assumed to be functions of temperature. The conductance term $G_{j_+}^n$ is evaluated at some appropriate location between nodes "j" and "j+1". This position is normally taken to be the midpoint between the two nodes. Equation (A-5) may be written as

$$C_{j}^{n} \frac{T_{j}^{n+1} - T_{j}^{n}}{\Delta t^{n}} = G_{j_+}^{n} (T_{j+1}^{n} - T_{j}^{n}) + G_{j_-}^{n} (T_{j-1}^{n} - T_{j}^{n}) + Q_{j}^{n}. \qquad \text{(A-8)}$$

This technique may be easily extended to multiple dimensions. The resulting equation can then be written in the following form.

$$\left(\frac{C_j^n}{\Delta t^n}\right) (T_j^{n+1} - T_j^n) = \sum_{i=1}^{N} G_{ij}^{n} (T_i^n - T_j^n) + Q_j^n. \qquad \text{(A-9)}$$

In this equation G_{ij}^n represents the conductance value between node "j" and an adjoining node "i". The summation ranges from one to N where N is the

total number of nodes connected to node "j". The resulting set of equations may be solved explicitly for the nodal temperatures at the new time T_j^{n+1} in terms of quantities that are known at the old time.

A forward time or explicit technique was used in the development of Equation (A-9). If a backward differencing technique is applied, an equation similar to Equation (A-9) is obtained:

$$\left(\frac{C_j^{n+1}}{\Delta t^n}\right)(T_j^{n+1} - T_j^n) = \sum_{i=1}^{N} G_{ij}^{n+1}\,(T_i^{n+1} - T_j^{n+1}) + Q_j^{n+1} \qquad \text{(A-10)}$$

However, this equation is implicit in nature in that the quantities T^{n+1} cannot be solved for directly. If the strictly explicit and implicit equations are linearly averaged, an equation known as a mid-difference or Crank-Nicholson type equation is obtained. This equation involves terms of the type C_j^{n+1} and G_{ij}^{n+1} that are functions of the nodal temperatures at the new times. Since these values will not change appreciably from one time to the next, the assumption made in CINDA-3G is that $C_j^{n+1} = C_j^n$, $G_{ij}^{n+1} = G_{ij}^n$, and $Q_j^{n+1} = Q_j^n$. The mid-difference equation solved by CINDA-3G is

$$\left(\frac{C_j^n}{\Delta t^n}\right)(T_j^{n+1} - T_j^n) = \sum_{i=1}^{N} G_{ij}^n \left\{1/2\,(T_i^{n+1} - T_j^{n+1}) + 1/2\,(T_i^n - T_j^n)\right\} + Q_j^n \,. \qquad \text{(A-11)}$$

The solution of the resulting set of simultaneous equations is obtained by an iterative technique that accounts for the sparsity of the coefficient matrix. When the solution has converged to within a prescribed convergence criterion the time is advanced.

A stability criterion that limits the maximum allowable time step size exists for the explicit technique. If Equation (A-9) is rearranged in the following form

$$T_j^{n+1} = \left(1 - \frac{\Delta t^n \sum_{i=1}^{N} G_{ij}^n}{C_j^n}\right) T_j^n + \left(\frac{\Delta t^n}{C_j^n}\right) \sum_{i=1}^{N} G_{ij}^n\, T_i^n + \left(\frac{\Delta t^n}{C_j^n}\right) Q_j^n \qquad \text{(A-12)}$$

only the behavior of the coefficients need be determined to determine the stability characteristics of the difference equation. By applying the maximum principle[A-2] to Equation (A-12) and for simplicity by letting $\alpha_j^n = \Delta t^n / C_j^n$ and $\beta_j^n = Q_j^n / C_j^n$, the following equation results:

$$|T_j^{n+1}| \le |(1 - \alpha_j^n \sum_{i=1}^{N} G_{ij}^n)|\,|T_j^n| + |\alpha_j^n| \sum_{i=1}^{N} |G_{ij}^n|\,|T_i^n| + \Delta t^n |\beta_j^n| .$$

The conductance and capacitance terms are positive and, therefore, all temperature coefficients are positive except possibly $(1 - \alpha_j^n \sum_{i=1}^{N} G_{ij}^n)$. If

$(1 - \alpha_j^n \sum_{i=1}^{N} G_{ij}^n)$ is assumed to be nonnegative, then

$$|T_j^{n+1}| \leq (1 - \alpha_j^n \sum_{i=1}^{N} G_{ij}^n)\,|T_j^n| + \alpha_j^n \sum_{i=1}^{N} G_{ij}^n\,|T_i^n| + \Delta t^n |\beta_j^n| . \quad \text{(A-13)}$$

The norms of the temperature and the source terms are defined as

$$||T^n|| = \max_j |T_j^n|$$

and

$$||\beta^n|| = \max_j |\beta_j^n| . \quad \text{(A-14)}$$

Equation (A-13) then becomes

$$|T_j^{n+1}| \leq (1 - \alpha_j^n \sum_{i=1}^{N} G_{ij}^n)\,||T^n|| + \alpha_j^n \sum_{i=1}^{N} G_{ij}^n\,||T^n|| + \Delta t||\beta^n||$$

$$\leq \left[1 - \alpha_j^n \sum_{i=1}^{N} G_{ij}^n + \alpha_j^n \sum_{i=1}^{N} G_{ij}^n\right]||T^n|| + \Delta t^n\,||\beta^n||$$

$$\leq ||T^n|| + \Delta t^n||\beta^n||. \quad \text{(A-15)}$$

Since Equation (A-15) holds for all j's then

$$||T^{n+1}|| \leq ||T^n|| + \Delta t^n||\beta^n||. \quad \text{(A-16)}$$

If $||T^{n+1}||$ can be shown to be uniformly bounded then stability of the difference equation is implied. Then

$$||T^{n+1}|| \leq ||T^{n-1}|| + \Delta t^{n-1}||\beta^{n-1}|| + \Delta t^n||\beta^n||$$

$$\leq ||T^o|| + \Delta t^o||\beta^o|| + \Delta t^1||\beta^1|| + \text{----} + \Delta t^1\,||\beta^n||. \quad \text{(A-17)}$$

If $K = \max_n ||\beta^n||$ then

$$||T^{n+1}|| \leq ||T^o|| + (\Delta t^o + \Delta t' + \text{---} + \Delta t^n)\,K. \quad \text{(A-18)}$$

Now $\sum_{i=1}^{n} \Delta t^i \leq t$ where t is a finite time. Therefore

$$||T^{n+1}|| \leq ||T^o|| + tK. \quad \text{(A-19)}$$

Since $||T^{n+1}||$ is uniformly bounded, stability of the difference equation is assured.

The assumption that $(1 - \alpha_j^n \sum_{i=1}^{N} G_{ij}^n)$ was positive was required in the analysis. Therefore, the stability requirement for Equation (A-9) is

$$1 - \frac{\Delta t^n \sum_{i=1}^{N} G_{ij}^n}{C_j^n} \geq 0$$

or

$$\Delta t^n \leq \frac{C_j^n}{\sum_{i=1}^{N} G_{ij}^n} . \qquad \text{(A-20)}$$

The stability of the Crank-Nickolson solution technique is know to impose no restrictions on the mesh size [A-3]. Thus, any size time step may be used in the computations providing rapid changes in boundary conditions are not passed over. In spite of the capability of using larger time step sizes, the implicit solution is slower than the explicit scheme because of the iterative technique required to solve the equations.

A-1. REFERENCES

A-1. J. D. Gaski, Chrylser Improved Numerical Differencing Analyzer for 3rd Generation Computers, Chrysler Corporation Technical Note TN-AP-287 (October 1967).

A-2. S. K. Godunov, V. S. Ryabenki, Theory of Difference Schemes, New York: Interscience Publishers, A Division of John Wiley & Sons, Inc. (1964) p 108.

A-3. R. D. Richtmyer and K. W. Morton, Difference Methods for Initial-Value Problems, New York: John Wiley & Sons (1967) 2nd ed. lnSci.

APPENDIX B

NUMERICAL SOLUTION OF FLUID ENERGY EQUATION -- EXPLICIT METHOD